Sequential Processivity and CAND1 Regulate SCF Ubiquitin Ligases

Thesis by

Nathan William Pierce

In Partial Fulfillment of the Requirements

for the Degree of

Doctor of Philosophy

California Institute of Technology

Pasadena, California

2012

(Defended November 10, 2011)

To my father Terry, my mother Lynne, my wife Terrell, and to myself, for not giving up on me.

Acknowledgments

There are many people to thank for help getting to this point. First, I would like to send my deepest regards to the teachers throughout my life who made science and learning fun and interesting. Second, I would like to thank the people who wrote my recommendation letters for graduate school including James Nelson, David K Stevenson, and Gerry Fuller. Without their guidance and support I would not be here. Third, I would like to thank Caltech itself for accepting me to graduate school. Despite getting interviews at several schools, I was only accepted to MIT and Caltech.

I want to thank my family and wife Terrell for constant support throughout these years. There are many people I have met at Caltech that deserve mention: This includes Gary Kleiger and Anj Saha for providing key support and discussions regarding the mechanisms of SCF ubiquitin ligases. Tara Gomez, Natalie Kolawa, Mike Rome, Kuang-Jung Chang, and Ruzbeh Mosadeghi for marching beside me in the trenches of graduate student life in the Deshaies lab. Eugene Lee for everything regarding Mass Spec. Willem den Besten for fantastic discussions and knowledge of molecular and cellular biology. Narimon Honarpour for a sunny disposition and great insight into future family life. Tsui-Fen Chou for great discussions regarding future scientific life. Rob Oania for always being there when I needed something for my experiments. Heenam Park and Geoff Smith for pouring fantastic gels throughout the years. Rati Verma for her limitless knowledge of the UPS field that she helped create. Daphne Shimoda for help with trying to decide on lunch for group meeting and trying to schedule the relentlessly busy Ray Deshaies. Senthil

Radhakrishnan for comic relief and straight answers. Dane Mohl for critical critiques of ideas on SCF mechanisms. Xin Zhang for serious science and hilarious lab manner. Peera Jaru-Ampornpan for always telling me to get back to work. Sowmya Chandrasekar, without whom I would never know what was going on. Thang Nguyen for adventures in step aerobics and zumba. Ishu Sarogi for her deep understanding of life's truer meanings. Kuang Shen for spicy food and spicy science. David Akopian for his philosophical grasp on this absurd reality. Adler Dillman for continued friendship down the hall. Aadel Chaudhuri for always keeping it real. Megan Dobro for several years of awesome skits at the bio retreat. Amy McMahon for support and friendship. Alex Nisthal for being my roommate. The Woods Hole Physiology course for fantastic summer in 2010. Beth Larimore for sending me her unpublished construct for Fbxw7 expression.

I would like to thank the entire Caltech faculty for putting up with me and my crazy ideas for skits at the annual bio retreat; Ellen Rothenberg and David Chan for making teaching highly enjoyable; Paul Sternberg for being on my committee; and Bill Dunphy for being the head of my committee, being a great teacher to work with, and writing me a recommendation for post-doc fellowships.

Most importantly I would like to thank my two advisors Ray Deshaies in the Division of Biology and Shu-ou Shan in the Division of Chemistry. Both are amazing mentors and all around brilliant scientists of the highest degree in their respective fields.

Abstract

The modular design of the multi-subunit SCF ubiquitin ligases allows for recognition of a diverse set of target proteins. However, the speed and complexity of the SCF ubiquitylation reaction have precluded direct experimental tests to understand how SCF complex formation is regulated and the pathway by which ubiquitin chains are generated. Herein we introduce new theoretical and experimental methodologies to address both limitations. First, a quantitative framework based on product distribution predicts that the really interesting new gene (RING) E3s SCF^{Cdc4} and $SCF^{\beta\text{-}TrCP}$ work with the E2 Cdc34 to build polyubiquitin chains on substrates by sequential transfers of single ubiquitins. Measurements with millisecond time resolution directly demonstrate that substrate polyubiquitylation proceeds sequentially. Second, we present a novel FRET assay that enables real-time measurements of binding dynamics of the SCF^{Fbxw7} complex. We find that the Cul1-associated protein CAND1 is able to actively remove Fbxw7/Skp1 from Cul1/Rbx1 by changing the dissociation rate of the complex a million-fold, yet CAND1 does not affect the assembly rate of SCF^{Fbxw7}. This activity is abolished when Cul1 is neddylated. Experiments show that CAND1 accelerates the rate at which multiple SCF complexes can form. Thus, CAND1 appears to function as an exchange factor. Lastly, several measurements reveal an extra step in the ubiquitylation pathway for yeast SCF that implies a substrate induced conformational change exists for Fbox proteins. These results present an unprecedented glimpse into the mechanism of RING ubiquitin ligases and their regulation by CAND1.

Contents

Chapter 1:

Introduction

In the past 30 years, the degradation of proteins through the ubiquitin proteasome system (UPS) has emerged as an essential process that governs a wide range of biological processes. As such, mutations in many of the basic UPS components are now understood to serve as the underlying molecular cause of several diseases and disorders. Understanding the fundamental mechanisms of how the UPS works gives promise for the development of future treatments.

Discovery of Ubiquitin

Results from early metabolic studies in rats revealed that protein turnover was extensive and rapid (Schoenheimer et al., 1939). Protein degradation was initially thought to occur exclusively in the lysosome, an intracellular compartment with destructively low pH that at the time was known to degrade proteins after endocytosis. However, several studies indicated that ATP was required for the specific degradation of certain types of abnormal proteins. This indicated, although it did not prove, that mechanisms existed outside the context of the lysosome that were responsible for protein catabolism. The beginnings of the UPS field can be traced back to the seminal work of Alfred Goldberg at Harvard Medical School. Goldberg and colleagues established a cell-free system in rabbit reticulocyte lysate that recapitulated the ATP-dependent degradation of hemoglobin upon mis-incorporation of the valine analog 2-amino-3-chlorobutyric acid (ClAbu) (Etlinger and Goldberg, 1977). Using this assay, the lab of Avram Hershko set out to find the enzymes that were responsible for this activity through biochemical fractionation of the lysate. The group discovered a small, heat-stable protein that was required for

activity (Ciechanover et al., 1978). The group of Art Haas quickly discovered that this protein was in fact ubiquitin, an abundant eukaryotic protein with unknown function that had been shown to become covalently linked to histone 2A (Wilkinson et al., 1980; Goldstein et al., 1975; Goldknopf and Busch, 1977). In a now famous paper, Hershko and Irwin Rose observed radiolabeled ubiquitin attachment to lysozyme and proposed that ubiquitin attachment to proteins served as an intermediate to the delivery of proteins to some unknown protease (Hershko et al., 1980). This served as the reason for the ATP dependence on protein degradation activity seen in the lysate.

The Ubiqutin Enzymes

In general, a sequential cascade of three enzymes carries out the transfer of mono-ubiquitin to target proteins and the synthesis of polyubiquitin chains: a ubiquitin activating enzyme (E1), a ubiquitin conjugating enzyme (E2), and a ubiquitin ligase (E3) (Figure 1.1) (Dye et al., 2007). The E1 enzyme uses ATP to catalyze the formation of an adenylate conjugate at the C-terminus of ubiquitin (Hershko et al., 1981). This high-energy intermediate is hydrolyzed to directly attach the E1 to ubiquitin through a thiolester linkage between an active site cysteine on the E1 and the C-terminus of ubiquitin (Haas et al., 1982). Almost all eukaryotic organisms have a single ubiquitin E1, with the exception of humans, which have two (Jin et al., 2007). Most organisms have around ten E2s. E2s interact directly with the E1 and the ubiquitin is transferred from the catalytic cysteine of the E1 to the catalytic cysteine of the E2.

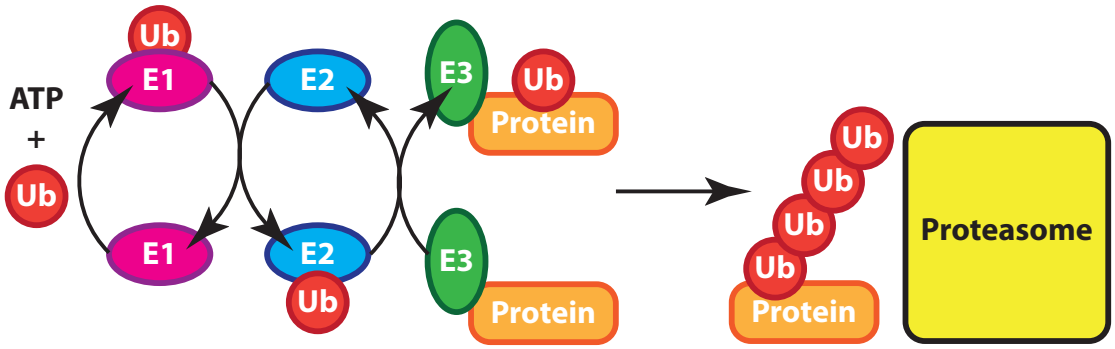

Figure 1.1 | The General Scheme for the UPS. Three enzymes work in succession to covalently attach ubiquitin and ubiquitin chains to target proteins: the ubiquitin activating enzyme (E1), the ubiquitin conjugating enzyme (E2), and the ubiquitin ligase (E3). The massive multi-subunit protease the proteasome recognizes ubiquitin chains through its receptors, leading to subsequent degradation.

E3 ligases are aptly named because they interact directly with the protein to be ubiquitylated. There are two main types of E3 ligases. HECT domain E3s accept ubiquitin from an E2 onto a catalytic cysteine, while RING (really interesting new gene) E3s catalyze the direct transfer of ubiquitin from an E2 to a lysine on a target protein (Petroski and Deshaies, 2005a). Cullin-RING ubiquitin ligases (CRLs) are the largest family of E3s and are typified by the SCF complexes, which in humans are composed of four proteins: the scaffold Cul1, the RING containing Rbx1, the adaptor Skp1, and a substrate binding protein that contains the Fbox motif (Deshaies and Joazeiro, 2009). 69 proteins in the human genome have Fbox motifs, and 42 have been shown to form SCF complexes (Lee et al., 2011). Although this modular design of SCF complexes allows for recognition of a diverse set of target proteins, how SCF complex formation is regulated remains unclear

The UPS highlights several modern aspects of the understanding of proteins in biology. First, post-translational modifications of proteins serve to expand and regulate the function of a wide array of cellular processes. Second, degradation of proteins is a mechanism of control critical for proper cellular signaling and function. This is pronounced by the vast array of diseases that are currently linked with the ubiquitin proteasome system.

Chapter 2:

Detection of Sequential Polyubiquitylation on a Millisecond Timescale*

*This chapter, first published in *Nature* in 2009, was written by Nathan W. Pierce, Gary Kleiger, Shu-ou Shan, and Raymond J. Deshaies.

Abstract

The pathway by which ubiquitin chains are generated on substrate via a cascade of enzymes consisting of an E1, E2, and E3 remains unclear. Multiple distinct models involving chain assembly on E2 or substrate have been proposed. However, the speed and complexity of the reaction have precluded direct experimental tests to distinguish between potential pathways. Here we introduce new theoretical and experimental methodologies to address both limitations. A quantitative framework based on product distribution predicts that the really interesting new gene (RING) E3s SCF^{Cdc4} and $SCF^{\beta\text{-}TrCP}$ work with the E2 Cdc34 to build polyubiquitin chains on substrates by sequential transfers of single ubiquitins. Measurements with millisecond time resolution directly demonstrate that substrate polyubiquitylation proceeds sequentially. Our results present an unprecedented glimpse into the mechanism of RING ubiquitin ligases and illuminate the quantitative parameters that underlie the rate and pattern of ubiquitin chain assembly.

Introduction

Attachment of a polyubiquitin chain with at least four ubiquitins linked together through their lysine 48 residue (Lys48) targets proteins to the proteasome for degradation (Thrower et al., 2000). A cascade of three enzymes carries out the synthesis of polyubiquitin chains: a ubiquitin activating enzyme (E1), a ubiquitin conjugating enzyme (E2), and a ubiquitin ligase (E3) (Dye et al., 2007). RING (really interesting new gene) E3s catalyze the direct transfer of ubiquitin from an E2 to a lysine on a target protein (Petroski and Deshaies, 2005a). SCF^{Cdc4} is the founding member of the largest family of E3s—the cullin-RING ubiquitin ligases (CRLs) that may comprise the majority of all human ubiquitin ligases (Petroski and Deshaies, 2005a). Thus, unraveling the mechanism of SCF will have broad functional ramifications for the preponderance of human E3s.

Different pathways for ubiquitin chain assembly by RING E3s have been envisioned based on indirect evidence. On the one hand, Cdc34-SCF ubiquitylates substrates bearing a single ubiquitin significantly faster than non-ubiquitylated substrates (Saha and Deshaies, 2008; Petroski and Deshaies, 2005b), suggesting that it processively builds polyubiquitin chains on substrates with an initial slow transfer of ubiquitin followed by rapid elongation into a Lys48-linked polyubiquitin chain. On the other hand, the E2 Ube2g2, a close relative of Cdc34, collaborates with the E3 gp78 to build a polyubiquitin chain on its active site cysteine that can be transferred en bloc to substrate (Ravid and Hochstrasser, 2007; Li et al., 2007). Various permutations of the en bloc mechanism have been entertained, in which the chain is built either from proximal to distal end or vice versa (Hochstrasser, 2006; Li

et al., 2009; Deshaies and Joazeiro, 2009). Due to the rapid speed of ubiquitin chain synthesis, intermediates that would reveal the underlying pathway cannot be kinetically resolved. Thus, it has not been possible to establish definitively the pathway of chain assembly for any RING E3. Here we introduce new theoretical and experimental methodologies to address both limitations.

Results

Quantitative analysis of product distribution

Processivity emerges from the relationships between reaction and dissociation rates for different product intermediates (Fersht, 1999). To quantify the processivity of SCF, we established an assay capable of simultaneously monitoring the concentrations of substrate and its different ubiquitylated product intermediates. Our assay consisted of an engineered phosphopeptide substrate derived from human Cyclin E1 (CycE) and purified *Saccharomyces cerevisiae* Cdc34-SCF^{Cdc4} (Saha and Deshaies, 2008; Petroski and Deshaies, 2005b; Nash et al., 2001). CycE was selected because it is a defined, chemically homogeneous substrate that binds with high affinity to the substrate-binding pocket of SCF^{Cdc4} (Nash et al., 2001; Orlicky et al., 2003). Moreover, intact Cyclin E is a substrate of SCF^{Cdc4} *in vivo* (Strohmaier et al., 2001) and the degron from CycE can support turnover *in vivo* of an engineered substrate, Sic1, from which the endogenous degrons have been eliminated (Nash et al., 2001). To examine the simplest system that recapitulated the processive behavior of Cdc34-SCF^{Cdc4}, we focused on single turnover reaction conditions containing an excess of SCF^{Cdc4} over radiolabeled CycE. We initiated reactions by combining two pre-incubated mixtures: the 'charged E2' mixture containing ubiquitin, E1, ATP, and Cdc34 was pre-incubated for two minutes to ensure the formation of saturating concentrations of Cdc34~ubiquitin thioesters (E2~Ub), and the 'substrate-ligase' mixture containing SCF and radiolabeled substrate was pre-incubated to ensure the formation of an enzyme-substrate complex. To maximize resolution of ubiquitin conjugates, the reaction products

were fractionated on long SDS-polyacrylamide gels. Consistent with previous assays performed with Sic1 (Petroski and Deshaies, 2005b), conjugation of the Nedd8 homologue Rub1 to the Cdc53 subunit of budding yeast SCF^{Cdc4} did not alter the ubiquitylation kinetics of CycE (Supplementary Figure A.1), and thus all subsequent SCF^{Cdc4} assays were performed with unmodified E3.

Under these reaction conditions, CycE was extensively polyubiquitylated by Cdc34-SCF^{Cdc4} within 30 seconds (reaction 1, Figure 2.1a), and products containing ≥ 6 ubiquitins were visible within 10 seconds (Supplementary Figure A.1). Thus, with the time resolution offered by manual mixing it was not apparent whether ubiquitin conjugates were formed by multiple sequential transfers of monoubiquitin or by en-bloc transfer of pre-formed chains. However, we reasoned that quantitative analysis of the length distribution of polyubiquitin chains attached to CycE during a single encounter with SCF might provide clues to the pathway of chain assembly. To determine the length distribution we carried out reactions with 1,000-fold excess chase of the unlabeled substrate peptide added to the 'charged E2' mixture (reaction 2, Figure 2.1a). Under these conditions, radiolabeled substrate pre-bound to SCF was rapidly ubiquitylated, but upon dissociation further ubiquitylation occurred at a significantly reduced rate due to competition from the chase peptide. To evaluate the effectiveness of the chase, we carried out a parallel reaction in which the chase peptide was added to the 'substrate-ligase' mixture prior to initiation (reaction 3, Figure 2.1a). The distribution of products in reaction 3 was subtracted from the distribution of products in reaction 2 at each time point (Supplementary Figure A.2)

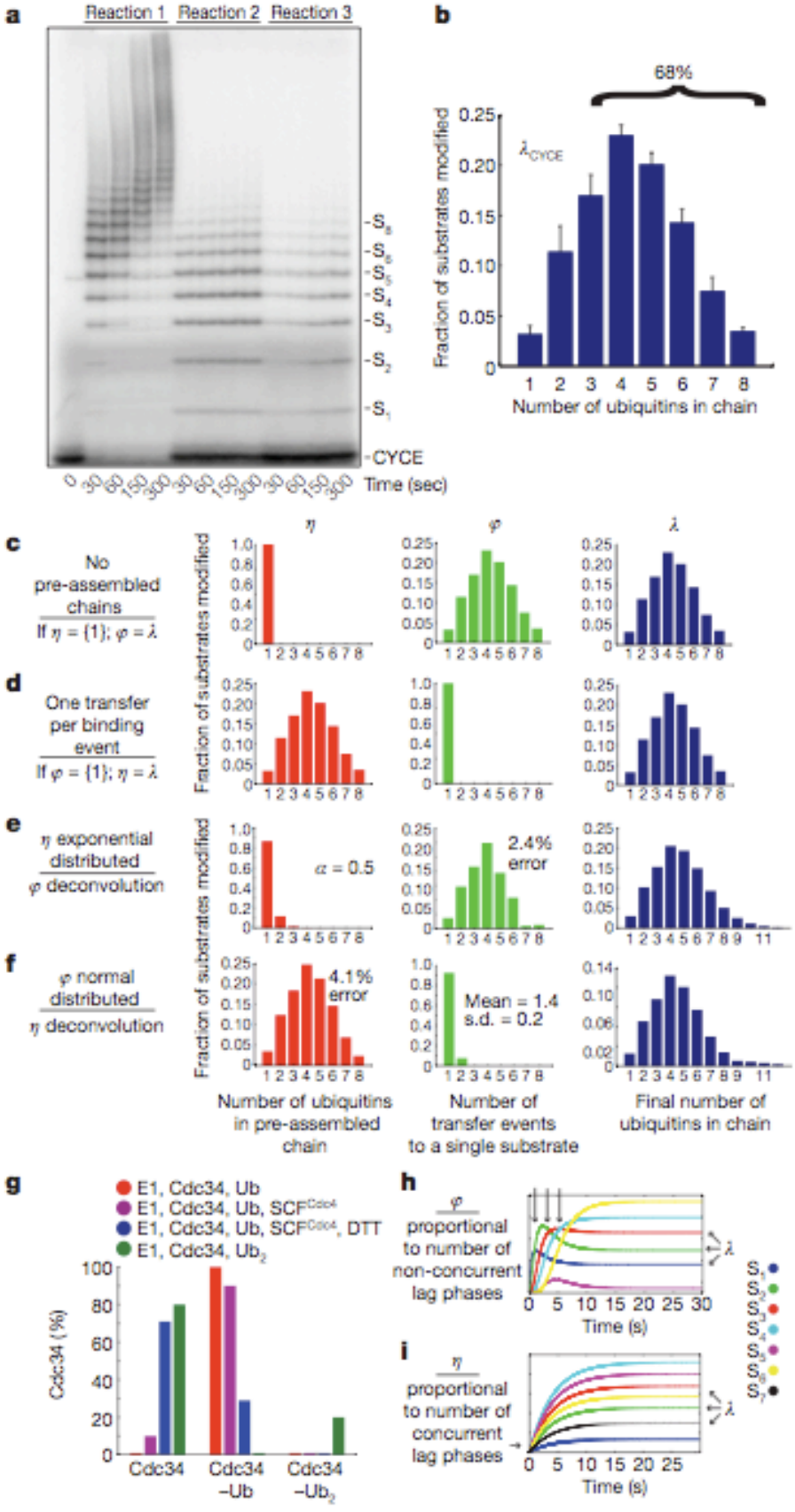
a
Reaction 1
Reaction 2
Reaction 3
S8
S7
S6
S5
S4
S3
S2
S1
CYCE
0 30 60 150 300 30 60 150 300 30 60 150 300
Time (sec)
b
68%
λCYCE
Fraction of substrates modified
Number of ubiquitins in chain
c
No pre-assembled chains
If η = {1}; φ = λ
d
One transfer per binding event
If φ = {1}; η = λ
e
η exponential distributed
φ deconvolution
α = 0.5
2.4% error
f
φ normal distributed
η deconvolution
4.1% error
Mean = 1.4
s.d. = 0.2
Number of ubiquitins in pre-assembled chain
Number of transfer events to a single substrate
Final number of ubiquitins in chain
g
E1, Cdc34, Ub
E1, Cdc34, Ub, SCFCdc4
E1, Cdc34, Ub, SCFCdc4, DTT
E1, Cdc34, Ub2
Cdc34 (%)
Cdc34
Cdc34 –Ub
Cdc34 –Ub2
h
φ
proportional to number of non-concurrent lag phases
Time (s)
i
η
proportional to number of concurrent lag phases
Time (s)

Figure 2.1 | Final product distribution for SCF^{Cdc4} and CycE. a, In reaction 1, pre-incubated ^{32}P-labeled CycE and SCF^{Cdc4} were added to the charged E2 mix. In reactions 2 and 3, excess unlabeled CycE was pre-incubated with charged E2 mix and labeled CycE, respectively. **b,** The single encounter polyubiquitin chain length distribution, λ_{CycE}. Error bars: +/- SD, n=3. **c,** If $\eta(1)=100\%$, then $\varphi=\lambda$. **d,** If $\varphi(1)=100\%$, then $\eta=\lambda$. **e,** Deconvolution of λ_{CycE} and exponentially distributed η. **f,** Deconvolution of λ_{CycE} and normal distributed φ. **g,** Mass spectrometry of Cdc34 thioesterified for 2' with indicated components. **h,** Simulated kinetics $\eta(1)=100\%$. **i,** Simulated kinetics $\varphi(1)=100\%$.

to yield the average distribution for substrate, λ (Figure 2.1b). Three main points were highlighted by these experiments. First, it is evident from reaction 2 that the single encounter reaction was complete within 30 seconds. Second, 72% of CycE encounters with SCF^{Cdc4} resulted in no ubiquitin modification (Figure 2.1a and Supplementary Figure A.2). Third, of those substrates that were modified, 68% of CycE acquired a polyubiquitin chain with 4 or more ubiquitins (Figure 2.1b).

We next sought to develop a quantitative framework to address whether the experimentally determined product distribution λ_{CycE} (Figure 2.1b) places constraints on the potential pathways of ubiquitin chain assembly. We considered three hypothetical situations. First, we imagined that only monoubiquitin was attached in each transfer event (Figure 2.1c, 'sequential'). Binning all of the transfer events per substrate gave the transfer distribution φ, which in this case would equal λ. Second, we imagined the other extreme in which only one transfer event occurs per substrate (Figure 2.1d, 'en-bloc'). In this case, λ would be equal to the distribution of pre-assembled polyubiquitin chains thioesterified to E2, which we named η. Third, we considered permutations that combined sequential and en bloc

transfers. For example, there are eight possible ways of making substrate modified with four ubiquitins (S_n, where n=4), including two transfers of diubiquitin or transfer of monoubiquitin followed by transfer of triubiquitin, etc. From this analysis, a key point emerged: regardless of the type of distribution we started with, the family of η and φ distributions compatible with λ_{CycE} (see Supplementary Methods) was restricted to extreme cases where either η or φ was nearly equal to λ_{CycE} (Figure 2.1e, f and Supplementary Figure A.3-7). Therefore, the vast majority of substrates either underwent one transfer per binding event or received a single ubiquitin per transfer event. Thus, accurately measuring product distribution constrained the number of possible pathways that could give rise to the reaction products we observed.

As a first test of whether ubiquitins were transferred all at once or sequentially, we measured the distribution of polyubiquitin chain lengths present on the active site of Cdc34 in the presence or absence of SCF^{Cdc4} by intact mass spectrometry. Cdc34 subjected to our standard 'charged E2' pre-incubation was completely converted to thioesters carrying a single ubiquitin (Cdc34~Ub; Fig. 1g and Supplementary Figure A.10). In the presence of SCF^{Cdc4}, 89% of Cdc34 was detected as Cdc34~Ub and 11% was unmodified; no Cdc34 species with more than one ubiquitin attached were detected. A control experiment run with diubiquitin confirmed that our assay was able to detect diubiquitin chains thioesterified to the active site of Cdc34 (Cdc34~Ub_2; Supplementary Figure A.11), but charging of Cdc34 with diubiquitin occurs with poor efficiency (~ 20%). Thus, our analysis of the product distribution λ coupled with measurement of the ubiquitin population

thioesterified to Cdc34 under our reaction conditions (an estimate of η) strongly predicts that Cdc34–SCF^{Cdc4} assembles ubiquitin chains on substrate primarily by sequential transfers of single ubiquitin molecules.

Millisecond kinetics of SCF

As a second, more definitive test of the hypothesis stated above, we sought to measure directly how the product distribution (Figure 2.1b) developed as a function of time. During a single encounter between a RING ubiquitin ligase and substrate, each intermediate should either undergo a transfer event or dissociate. If monoubiquitin is composed 100% of η as in Figure 2.1c, the products of the reaction should appear sequentially in time starting with S_1 and followed by S_2, then S_3, etc. Thus, the appearance of each sequential product should be delayed by a 'lag' phase (Figure 2.1h). In contrast, if a single transfer composed 100% of φ as in Fig. 1d, then the pattern of ubiquitin chains attached to substrate at the earliest time-points should reveal the distribution of pre-assembled chains thioesterified to Cdc34 (Fig. 1i). Thus, products of increasing mass should accumulate sequentially if chain synthesis is sequential, but should accumulate contemporaneously if chains are transferred en bloc. Therefore, with sufficient time resolution a single encounter experiment would provide definitive data to distinguish between the alternative models. To achieve the necessary time resolution, we performed our single encounter reactions on a quench flow apparatus that allowed us to take measurements on a time scale ranging from 10 milliseconds to 30 seconds (Figure 2.2a). To facilitate quantification of S_2 and S_5 in the CycE reaction, the same reaction

from Figure 2.2a was fractionated on a gel with different resolving capabilities (Supplementary Figure A.12). Three major conclusions arose from these experiments. First, the product CycE–Ub (S_1) was formed starting at the earliest

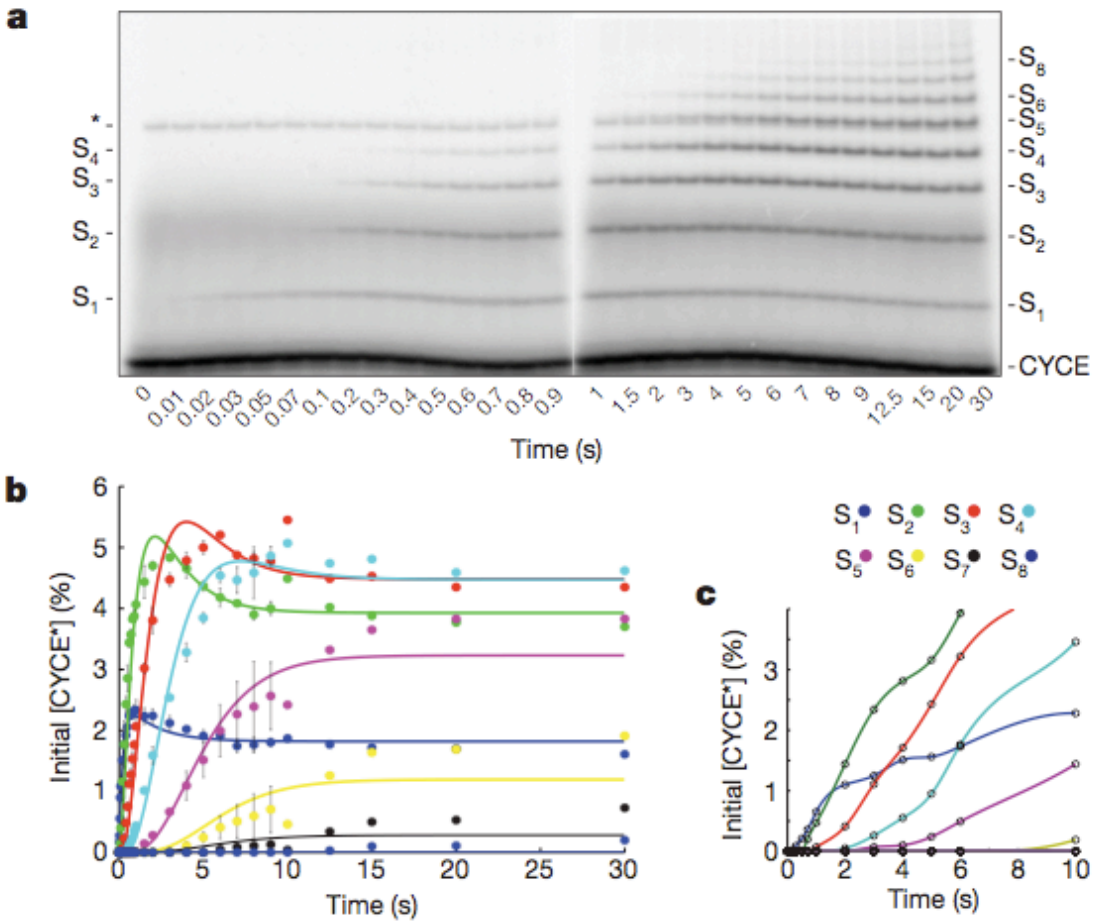

Figure 2.2 | Millisecond kinetics of a single encounter reaction reveal sequential processivity. **a,** To achieve millisecond temporal resolution CycE reactions were performed on a quench flow apparatus and products were evaluated by SDS-PAGE and phosphorimaging. The reaction scheme matched reaction 2 of Figure 2.1a. The asterisk marks a contaminant. S_n refers to CycE modified with n ubiquitins. **b,** Quantification shows successively longer lag phases for each additional ubiquitin added in the chain. The data was fit using closed form solutions refined by global regression analysis to a model with η=1. The error bars represent the range of values, n=2.

time points (10-20 milliseconds) without a lag phase, indicating that E2~Ub binding to SCF was rapid. This is consistent with stopped-flow measurements carried out with $SCF^{b\text{-}TrCP}$ and hCdc34 (Kleiger et al., 2009). Second, each new ubiquitylated product appeared sequentially with non-concurrent lag phases (Figure 2.2a, b and Supplementary Figure A.12). Third, the early reaction products S_1-S_3 'overshot' their final levels, indicating that these reaction intermediates serve as templates for the formation of subsequent products, supporting the model that polyubiquitin chains are built from multiple transfer events (Supplementary Figure A.16). Combined with the constraints on η and φ calculated above as well as our direct evaluation of the Cdc34~Ub pool (Figure 2.1g), these data demonstrate that the underlying kinetic mechanism of our system was principally derived from sequential transfers of single ubiquitins.

To ensure that our conclusions were not an artifact of the reaction design, we changed the order of addition in our reactions. SCF^{Cdc4} was pre-incubated with the 'charged E2' mixture for 2 minutes (in which case 89% of Cdc34 is present in thioesterified form; Figure 2.1g) and reactions were initiated by combining with radiolabeled CycE. Products appeared following non-concurrent lag phases of increasing duration (Figure 2.2c), analogous to that observed when the reaction was initiated by addition of Cdc34~Ub to CycE prebound to SCF^{Cdc4} (Figure 2.2a). Thus, regardless of whether CycE first encountered Cdc34~Ub–SCF or Cdc34~Ub encountered CycE–SCF, single ubiquitins were transferred to substrate in a sequential manner. Interestingly, reactions initiated by addition of CycE were

delayed compared with those initiated by addition of Cdc34~Ub, indicating that Cdc34~Ub productively associates with SCF^{Cdc4} faster than does CycE.

$SCF^{\beta\text{-}TrCP}$ is sequentially processive

We next sought to test whether the sequential processive chain assembly we observed for SCF^{Cdc4} is unique or illuminates a general principle of SCF ubiquitin ligase mechanism. To address this issue, we evaluated ubiquitylation of a phosphopeptide derived from β-Catenin (β-Cat) by its cognate E2-E3 complex, hCdc34 and human $SCF^{b\text{-}TrCP}$. Nedd8 conjugated E3 (N8-$SCF^{\beta\text{-}TrCP}$) was used for these experiments, because prior work demonstrated a potent stimulation of β-Cat ubiquitylation upon Nedd8 conjugation (Saha and Deshaies, 2009). As was seen with CycE–SCF^{Cdc4}, β-Cat was rapidly modified by N8-$SCF^{\beta\text{-}TrCP}$ and it was not possible to resolve intermediates in chain assembly by manual mixing[4] (Figure 2.3a). Quantification of product distribution $\lambda_{\beta\text{-}Cat}$ revealed that 6% of β-Cat molecules were modified in a single encounter with N8-$SCF^{\beta\text{-}TrCP}$, of which 85% received ≥ 4 ubiquitins (Figure 2.3b and Supplementary Figure A.2). Distribution analysis of $\lambda_{\beta\text{-}Cat}$ (Figure 2.3c) and kinetic resolution of β-Cat ubiquitylation by quench-flow (Figure 2.3d, e) revealed sequential appearance of intermediates analogous to those observed with CycE ubiquitylation by SCF^{Cdc4}.

Although the general behavior of SCF^{Cdc4} and N8-$SCF^{\beta\text{-}TrCP}$ were similar, the enzymes differed in the extent to which they converted bound substrate to product and elongated ubiquitin chains. Using a kinetic model in which monoubiquitin composed 100% of η, we were able to employ methods borrowed from the study of

nucleic acid polymerases (Kati et al., 1992) to extrapolate estimates for the individual reaction and dissociation rate constants from our single encounter quench-flow experiments (Figure 2.4, Supplementary Figure A.13-15).

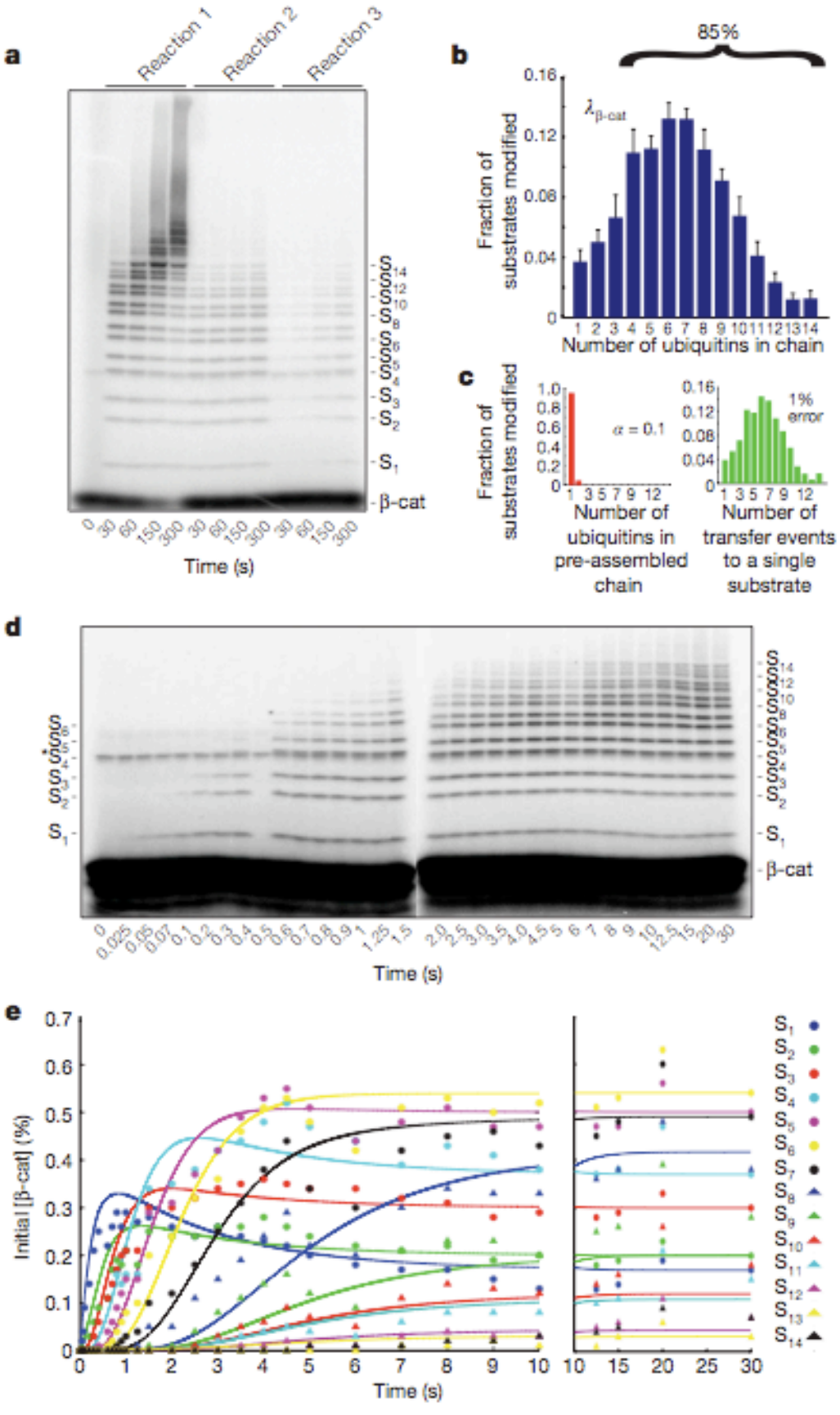
a
Reaction 1
Reaction 2
Reaction 3
S14
S12
S10
S8
S6
S5
S4
S3
S2
S1
β-cat
0 30 60 150 300 30 60 150 300 30 60 150 300
Time (s)
b
85%
0.16
0.12
0.08
0.04
0
λβ-cat
Fraction of substrates modified
1 2 3 4 5 6 7 8 9 10 11 12 13 14
Number of ubiquitins in chain
c
Fraction of substrates modified
1.0
0.8
0.6
0.4
0.2
0
α = 0.1
1 3 5 7 9 12
Number of ubiquitins in pre-assembled chain
0.16
0.12
0.08
0.04
0
1%
error
1 3 5 7 9 12
Number of transfer events to a single substrate
d
S8
S5
S4
S3
S2
S1
S14
S12
S10
S8
S6
S5
S4
S3
S2
S1
β-cat
0 0.025 0.05 0.07 0.1 0.2 0.3 0.4 0.5 0.6 0.7 0.8 0.9 1 1.25 1.5 2.0 2.5 3.0 3.5 4.0 4.5 5 6 7 8 9 10 12.5 15 20 30
Time (s)
e
Initial [β-cat] (%)
0.7
0.6
0.5
0.4
0.3
0.2
0.1
0
0 1 2 3 4 5 6 7 8 9 10
10 15 20 25 30
Time (s)
S1
S2
S3
S4
S5
S6
S7
S8
S9
S10
S11
S12
S13
S14

Figure 2.3 | Human Cdc34-SCF$^{β\text{-}TrCP}$ is sequentially processive. a, same as Figure 2.1a, except that human Cdc34 and Nedd8-conjugated SCF$^{b\text{-}TrCP}$ were assayed with ^{32}P-labeled b-Cat substrate. **b,** Product distribution ($l_{b\text{-}Cat}$) was quantified as in Figure 2.1b. Error bars: +/- SD, n=3. **c,** The Poisson distribution of φ using $\lambda_{\beta\text{-}Cat}$ that deviated the most from φ(1)=100% within our set error bounds with α=0.2. **d,** β-Cat reactions with the scheme of reaction 2 (Figure 2.1a) performed on a quench flow apparatus. **e,** Quantification shows successively lengthening lag phases for each additional ubiquitin added in the chain. The data was fit as in Figure 2.2b.

Discussion

Functional implications of our model

The model shown in Figure 2.4 reveals the kinetic basis of processive polyubiquitin chain synthesis by budding yeast Cdc34-SCF^{Cdc4} and human Cdc34-SCF$^{β\text{-}TrCP}$ and accounts for the differences in their behavior. Most encounters of substrate and SCF are unproductive because k_{off} is faster than k_{Ub1}. This is particularly exaggerated for b-Cat owing to its low value for k_{Ub1}. Once a single ubiquitin is attached, the majority of substrates are committed to polyubiquitylation due to the drastic increase in k_{Ub2} relative to a nearly constant k_{off}. This gives rise to the high percentage of modified substrates with four or more ubiquitins in their chain (68% for CycE and 85% for β-Cat). The overall chain length is limited by the progressive decrease in transfer rates (k_{Ubn}) as the chain becomes longer matched against the relatively constant rate at which product intermediates dissociate. This reduction in transfer rate most likely arises because the distal end of the flexible chain samples a progressively larger volume as it increases in length (Petroski et al.,

2006). The longer chains on β-Cat are a result of a less dramatic decline in k_{Ubn} after the second

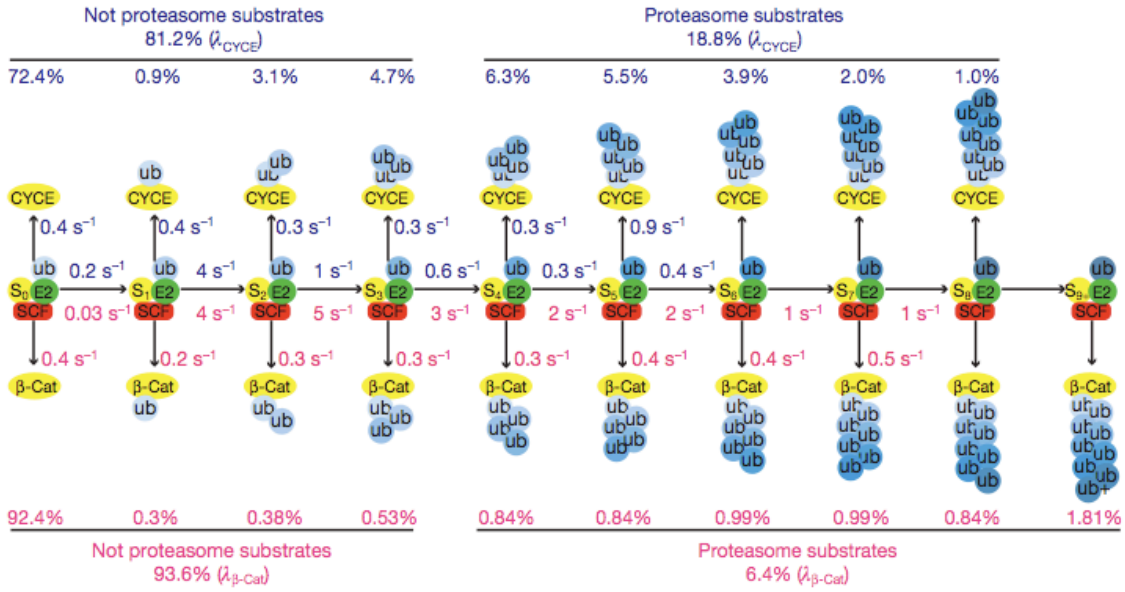

Figure 2.4 | Kinetic basis for Cdc34-SCF processivity. The millisecond kinetics of a single encounter reaction were fit to a sequential model revealing estimates for individual transfer and dissociation rates for each intermediate in the generation of polyubiquitylated CycE (blue numbers) and β-Cat (red numbers) products. The percentages listed above or below each product were the percentages from the final product distributions (λ) shown in Figures 2.1b and 2.3b.

ubiquitin is attached. We do not understand the basis for this difference. Meanwhile, the constant rate of dissociation for both CycE and β-Cat implies that ubiquitin chains of increasing length do not change the intrinsic affinity of these substrates for SCF.

Casual inspection of our model suggests that modest changes in the ratio k_{Ub1}/k_{off} for the first step would substantially alter the fraction of substrate that acquires a chain of ≥ 4 ubiquitins in a single encounter with SCF. This in turn

provides a simple basis for SCF to modulate a substrate's degradation half-life (i.e., the larger k_{off} is or smaller k_{Ub1} is, the lower the probability that a substrate is modified in a single encounter with SCF, which would translate to a longer half-life). Comparison of CycE and b-Cat, which have distinct k_{Ub1}/k_{off} ratios, underscores how the efficiency and pattern of substrate ubiquitylation can be tuned by these parameters. Despite these differences, it is remarkable how similar the reaction parameters are for two different enzymes from organisms separated by over 1 billion years of evolution. In both cases k_{off} was $\sim$ 0.4 sec^{-1} and the fastest rate of ubiquitin chain elongation was 4-5 sec^{-1}. This suggests that true substrates are tuned to dissociate within a few seconds and that a transfer rate of 5 sec^{-1} may be imposed by a conserved rate-limiting step. It will be of great interest to determine what molecular event enforces this speed limit.

We conclude that polyubiquitin chains are built on SCF substrates by sequential transfers of single ubiquitins. We establish a mechanistic framework that can be applied to other CRLs and RING ubiquitin ligases to obtain individual rate constants for substrate dissociation and ubiquitin transfer at each step in the process of chain assembly. Our model indicates that the processivity, efficiency, and pattern of ubiquitylation is governed by the sharp discontinuity in rates between the first transfer and subsequent transfers, contrasted with the shared dissociation rate among substrate and product intermediates.

Methods

Methods summary

Proteins

CycE and β-Cat phosphopeptide were purchased from New England Peptide. Ubiquitin and K48 diubiquitin were purchased from Boston Biochem. Uba1 and SCF^{Cdc4} were prepared and purified as described (Petroski and Deshaies, 2005b). Full-length yeast Cdc34 was purified as described (Feldman et al., 1997). His7-Rub1 was purified from *E. coli* inclusion bodies (Saha and Deshaies, 2008) and human E1, UbcH3B (hCdc34), and Nedd8-$SCF^{β\text{-}TrCP}$ were prepared and purified as described (Saha and Deshaies, 2008). Yeast Ubc12 and Ula1–Uba3 were purified as described (Kamura et al., 1999). Rub1, Ubc12, Ula1–Uba3, and ATP were incubated with immobilized SCF^{Cdc4} to make Rub1-conjugated SCF^{Cdc4}. PKA was purchased from New England Biolabs.

Ubiquitylation assay

CycE (200 nM) or β-Cat (2 μM) was incubated with g-[^{32}P]-ATP (132 nM) and PKA for 45 minutes at 30°C to make radiolabeled CycE or β-Cat. Yeast ubiquitylation reactions contained ATP (2 mM), ubiquitin (60 μM), Uba1 (0.8 μM), Cdc34 (10 μM), SCF^{Cdc4} (150 nM), and radiolabeled CycE (10 nM). Human ubiquitylation reactions contained ATP (2 mM), ubiquitin (60 μM), E1 (1 μM), Cdc34 (10 μM), $SCF^{β\text{-}TrCP}$ (500 nM), and radiolabeled β-Cat (100 nM). As indicated, single encounter reactions contained an unlabeled CycE chase (10 μM) or β-Cat chase (100 μM). Millisecond reactions were performed on a quench flow apparatus (Kintek RQF-3 Rapid Quench

Flow). Reactions contained a buffer previously described (Petroski and Dehsaies, 2005c) at 23°C. Reactions were quenched with SDS-PAGE buffer with βME and run on 20 cm 5-20% tricine gels (CycE) or Glycine gels (β-Cat) that were quantified with a phosphor screen (Molecular Devices). Thioester formation assays contained Cdc34 (10 μM), Uba1 (1 μM), ATP (2 mM), ubiquitin or K48 diubiquitin (15 μM), and SCF^{Cdc4} (100 nM), as indicated. After 2 minutes, reactions were stopped with excess 5% acetic acid and analyzed on an Agilent LC-MSD.

Analysis

Deconvolutions and regression were performed in Matlab. Global fitting was performed with KinTek Global Kinetic Explorer. Mass spec data was processed using the Chemstation software package.

Full Methods

RDB 2289 with pGEX2-T His7-Rub1 was made by cloning a His7 tag in place of the GST tag in RDB 1436. To make Rub1-conjugated SCF^{Cdc4}, the procedure for isolating SCF^{Cdc4} was modified (Petroski and Deshaies, 2005c). Instead of eluting SCF^{Cdc4} from Py conjugated protein A beads after washing, 50 μM Rub1, 10 μM Ubc12, 1 μM Ula1–Uba3, and 2 mM ATP were incubated together overnight. The beads were washed before elution.

For all reactions, gels were dried and exposed to Phosphor screens (Molecular Dynamics). Images were scanned and then quantified in ImageQuant using a rolling ball background subtraction. For each lane, every band was quantified as a percent of the total signal in all bands.

The relationship between η, φ, and λ was mathematically analogous to the probability of the sum of multiple dice throws. However, the probability of throwing each number on the dice was a weighted normalized distribution (analogous to η) and the number of throws was also a weighted normalized distribution (analogous to φ). A distribution that is normalized sums to 1. Thus, λ equaled the weighted sum of multiple discrete convolutions of η with itself as governed by φ, as shown by example in Supplementary Figure A.3. Knowledge of λ and η allowed us to calculate φ by multiple weighted deconvolutions, as shown by example in Supplementary Figure A.4. This was true for calculating η from λ and φ, as shown by example in Supplementary Figure A.5a. If we assigned a distribution to η, we determined φ by deconvolutions with λ, and vice versa. Considering normalized distributions of η that only contain η(1) and η(2), exponential distributions, poisson distributions, and normal distributions, we varied parameters over a wide range and performed deconvolutions, as shown by example in Supplementary Figure A.5b. An exponential distribution is described by a single parameter, here called α. A poisson distribution is also described by a single parameter, here called α. The normal distribution is described by two parameters, the mean and the standard deviation (SD). Parameters were varied starting at 0 and increasing by step sizes of 0.1 until parameters equaled 10. For the normal distribution, each value of the mean was held constant while the SD was varied. We sought the distribution which deviated most from η(1)=100% whose φ did not contain values > 1 or < 0, and that when convoluted with φ, the sum of λ fell within 0.95 and 1.05, or an error rate of ± 5% was found. This was repeated for φ. These distributions are shown in

Supplementary Figures A.6 and A.7. Random distributions were also considered (data not shown).

For mass spectrometry analysis, Uba1 (1 μM), Cdc34-Δ270 (10 μM), and ubiquitin or K48 linked di-ubiquitin (15 μM, Boston Biochem) were incubated for 2 minutes in reaction buffer (30 mM Tris, pH 7.5, 100 mM NaCl, 5 mM $MgCl_2$, 2 mM DTT, and 2 mM ATP) in a volume of 10 μl, both in the presence and absence of SCF (100 nM). Reactions were quenched by the addition of 90 μl 5 % acetic acid. Quenching was verified by an order of addition reaction where E1 was left out of the initial incubation and was added following quenching. This resulted in 100% quenching of the thioester charging reaction. Separation of E2 thioesters in the presence of SCF was accomplished by the addition of 100 mM DTT after the 2 minute incubation period. The DTT was incubated with the reaction mixture for 5 minutes, followed by the addition of 90 μl of 5 % acetic acid. Detection of proteins was carried out on an Agilent LC-MSD (Agilent, Palo Alto, CA). Mass spectra were acquired in positive-ion mode, scanning from 500 to 1700 m/z. The electrospray voltage was set to 4 kV and the gas temperature in the spray chamber was maintained at 350°C. A stationary phase, Zorbax 300SB C3 150×2.1-mm column was used for separation (Agilent; Bodman, Aston, PA). Mobile phase A was 0.2% formic acid and mobile phase B was 0.2% formic acid, 10% methanol, and 90% acetonitrile. The flow rate was 0.200 ml/min. After a 25 min delay, the effluent was directed into the mass spectrometer. Linear gradients started with 5% mobile phase B and finished at 95% from 25 – 50 min. Data were processed using the chemstation software package. The sequence of yeast Cdc34-Δ270 contains the

amino acids from positions 1 to 270 of the yeast Cdc34 sequence followed by the sequence ARPLHHHHHH, yielding a theoretical molecular mass of 32,245 Daltons. The theoretical mass of Cdc34-Δ270 thioesterified with ubiquitin (40,792) was calculated by summing the masses of Cdc34-Δ270 (32,245) and ubiquitin (8,565) and subtracting the mass of a water molecule, which is lost during formation of the thioester bond.

For CycE global fitting with KinTek Global Kinetic Explorer, the average of two independent experiments was fit to a model with $\eta=1$, and the fit for k_1 through k_4 used the normalized option, while the rest of the rate constants did not. For β-Cat global fitting, rate constants were fit without normalization. To improve fitting, neighboring rate constants were constrained by the end point.

Chapter 3:

CAND1 Functions as an Fbox Exchange Factor

Abstract

The modular design of the multi-subunit SCF ubiquitin ligases allows for recognition of a diverse set of target proteins. However, how SCF complex formation is regulated remains unclear. Cullin-associated and neddylation-dissociated protein 1 (CAND1) is a Cul1-associated protein that has been reported to inhibit SCF complex formation. Nonetheless, the function of CAND1 remains elusive given the lack of a mechanistic framework for each of its reported activities. Here we present a novel FRET assay that enables real-time measurements of binding dynamics of the SCF^{Fbxw7} complex. We find that CAND1 is able to actively remove Fbxw7/Skp1 from Cul1/Rbx1 by changing the dissociation rate of the complex a million-fold, yet CAND1 does not affect the assembly rate of SCF^{Fbxw7}. This activity is abolished when Cul1 is neddylated. Experiments show that CAND1 accelerates the rate at which multiple SCF complexes can form. Thus, CAND1 appears to function as an exchange factor. Our results serve as a basis to resolve the function of CAND1 *in vivo*.

Introduction

Three enzymes work in succession to covalently attach ubiquitin and ubiquitin chains to target proteins: a ubiquitin activating enzyme (E1), a ubiquitin conjugating enzyme (E2), and a ubiquitin ligase (E3) (Dye and Schulman, 2007). The proteasome, a massive multi-subunit protease, recognizes and degrades proteins attached with lysine 48 linked polyubiquitin chains containing at least four ubiquitins (Thrower et al., 2000). Cullin-RING ubiquitin ligases (CRLs) are the largest family of E3s and are typified by the SCF complexes, which in humans are composed of four proteins: the scaffold Cul1, the RING containing Rbx1, the adaptor Skp1, and a substrate binding protein that contains the Fbox motif (Petroski and Deshaies, 2005a). 69 proteins in the human genome have Fbox motifs, and 42 have been shown to form SCF complexes (Lee et al., 2011). Although this modular design of SCF complexes allows for recognition of a diverse set of target proteins, how SCF complex formation is regulated remains unclear.

Cullin-associated and neddylation-dissociated protein 1 (CAND1) was originally isolated as a Cul1 associated protein whose binding was mutually exclusive with the Fbox/Skp1 sub-complex (Liu et al., 2002; Zheng et al., 2002). CAND1's dissociation from Cul1/Rbx1 was coupled to the attachment of the ubiquitin-like protein Nedd8 to lysine 720 of Cul1 (Liu et al., 2002; Zheng et al., 2002). Neddylation of Cul1 activates SCF complexes by inducing a major conformational rearrangement in Cul1 and stimulates ubiquitin transfer from associated E2s to Fbox-bound target substrates (Saha and Deshaies, 2008; Duda et

al., 2008). *In vitro*, CAND1 acts as an inhibitor of CRL ubiquitylation and neddylation (Liu et al., 2002; Zheng et al., 2002; Siergiejuk et al., 2009). For these reasons, CAND1 was recognized as a negative regulator of SCF complex assembly. However, genetic evidence indicates that CAND1 acts as a positive regulator of CRL function *in vivo*. First, knock down of CAND1 by siRNA stimulates assembly of $Cul3^{Keap1}$ but reduces its ability to target Nrf2 for degradation (Lo, Hannink 2006). Second, siRNA against CAND1 stabilizes the SCF^{Skp2} substrate p27 (Zheng et al., 2002). Lastly, mutations in CAND1 in plants disrupt auxin and gibberellin signaling through stabilization of the SCF^{Tir1} substrate IAA7 and the SCF^{SLY1} substrate RGA, respectively (Chuang et al., 2004; Feng et al., 2004). These observations gave rise to the idea that CAND1-mediated CRL adaptor recycling was crucial for proper CRL function (Liu et al., 2002; Cope and Deshaies 2003; Schmidt et al., 2009; Zhang et al., 2008). Furthermore, the role of CAND1 was envisioned to be coupled to cycles of neddylation and de-neddylation in which CAND1 sequesters a substantial fraction of naked Cul1/Rbx1 devoid of Fbox/Skp1 and Nedd8 (Deshaies and Cope, 2003). However, a recent analysis of the CRL network *in vivo* found that in the absence of neddylation CAND1 does not sequester Cul1/Rbx1 away from Fbox/Skp1 complexes (Bennett et al., 2010).

In order to reconcile the above observations, we have constructed the first kinetic framework for the assembly of a CRL complex *in vitro* using a novel FRET assay that enables real-time measurements of SCF^{Fbxw7} binding dynamics. CAND1's perturbations of these dynamics reveal that CAND1 acts as a Nedd8-dependent Fbox exchange factor. Armed with this knowledge, we establish a biochemical assay

involving multiple Fboxes that reconstitutes the activator function of CAND1 *in vitro* with pure components. Our biochemical results show for the first time that CAND1 is sufficient for CRL adaptor cycling *in vitro* and that this activity leads directly to CAND1-mediated stimulation of CRL ubiquitin ligase activity. Further, CAND1's exchange factor activity represents a novel form of regulation for protein-protein interactions that thus far has only been seen for protein-small-molecule interactions, such as the GEFs.

Results

Intrinsic assembly properties of SCF^{Fbxw7}

To characterize the assembly properties of SCF complexes, we developed a real-time assay based on FRET that monitors the binding dynamics between the sub-complexes of Fbox/Skp1 and Cul1/Rbx1. The C-terminus of the Fbox protein Fbxw7 was fused to the peptide sequence LPETGG and co-expressed recombinantly with Skp1. After purification, we reacted the complex with the trans-peptidase enzyme Sortase in the presence of the peptide GGGGK-TAMRA, producing Fbxw7 covalently labeled with TAMRA (Popp et al., 2009). The trans-peptidation reaction was efficient and did not compromise ubiquitylation activity (Supplementary Figure B.1a). We observed FRET between Fbxw7-TAMRA/Skp1 and Cul1 fused N terminally to cyan fluorescent protein (CFP) co-expressed with Rbx1 (Figure 3.1a). The rate of complex assembly was determined by monitoring the changes of donor Cul1 NTD CFP/Rbx1 fluorescence when mixed with varying concentrations of Fbxw7 TAMRA/Skp1 in a stop flow apparatus. The change in signal was fit to single exponential curves (Figure 3.1b). The change in the observed rate of the reaction as a function of acceptor concentration revealed a fast binding rate of 4×10^{6} M^{-1} s^{-1} (Figure 3.1c). The FRET observed in our assay could be chased away by excess non-fluorescent Fbox/Skp1 (Figure 3.1d). Using this chase assay, we measured a dissociation rate for SCF^{Fbxw7} of 9×10^{-7} s^{-1} or 0.5 $week^{-1}$ (Figure 3.1e). These measurements revealed an extraordinarily tight complex with a K_d of 2×10^{-13} M (200 fM). Neddylation of Cul1 did not affect the FRET efficiency in our assay, the association rate, nor the dissociation rate of SCF complex assembly (Figure 3.1c &

Supplemental Figure B.1b-d). To extend our finding to other SCF complexes we attempted to make FRET assays using a similar strategy for Skp2 and β-TrCP, but were unsuccessful (data not shown). In lieu of direct binding data, we designed an assay that used Fbxw7-TAMRA/Skp1 as the chase and monitored gain of FRET (Supplemental Figure B.1e). An upper limit of 5 x 10^{-5} s^{-1} for the dissociation rate was found for $SCF^{\beta\text{-}TrCP}$ (Fig. 1f).

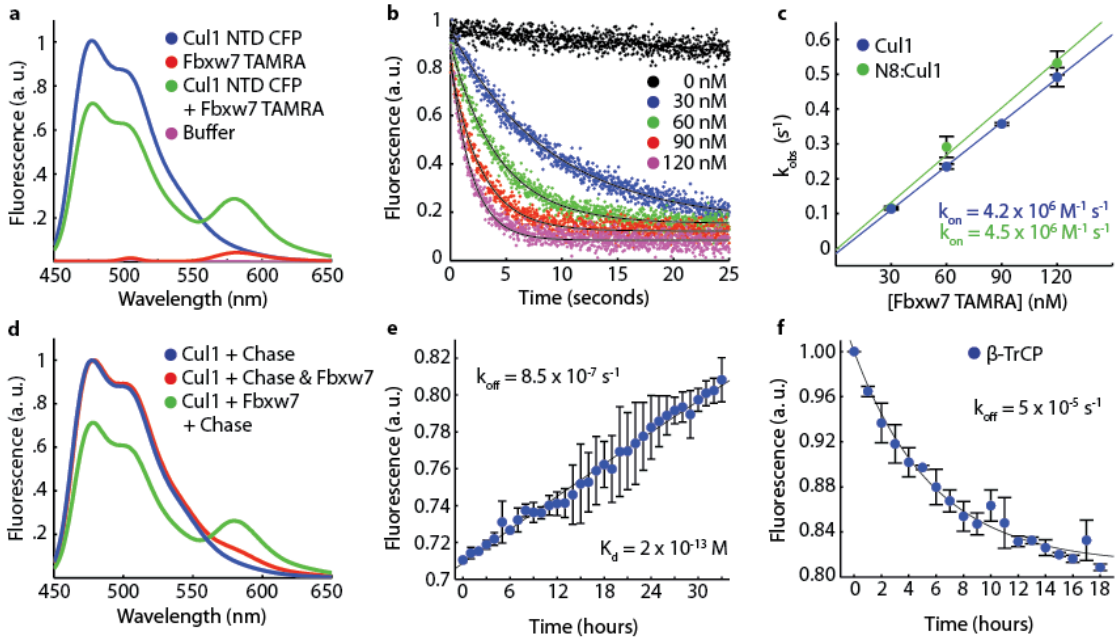

Figure 3.1 | FRET Reveals Properties of SCF Assembly. a, Fluorescence emission spectra from excitation at 430 nm of 70 nM Cul1 NTD CFP/Rbx1, 70 nM Fbxw7-TAMRA/Skp1, a mixture of the two, or buffer alone reveals FRET with 30% efficiency upon complex formation. Normalized to peak donor emission at 478 nm. **b,** The change in donor fluorescence versus time in a stop flow apparatus with 5 nM Cul1 NTD CFP/Rbx1 and varying concentrations of Fbxw7 TAMRA/Skp1. Signal changes were fit to single exponential curves. **c,** The rate of signal change in b versus the concentration of Fbxw7 TAMRA/Skp1. Fitting the data to (k_{obs} = k_{on}*[Fbxw7] + k_{off}) gave k_{on} of 4 x 10^6 M^{-1} s^{-1} regardless of Cul1's neddylation status. Error bars: +/- SD, n≥3. **d,** 700 nM Skp2/Skp1 (chase) competes FRET away if pre-incubated with 70 nM Fbxw7 TAMRA/Skp1 before, but not after addition of 70 nM Cul1

NTD CFP for 5 min. **e,** Fluorescence emission at 478 nm versus time after addition of chase to pre-incubated Cul1 NTD CFP/Rbx1 and Fbxw7 TAMRA/Skp1 normalized to peak donor emission in d. Single exponential fit with a fixed end point of 1 gave k_{off} of 8.5 x 10^{-7} s^{-7}. K_d is thus 2 x 10^{-13} M. Error bars: +/- SD, n=3. **f,** Fluorescence emission at 478 nm versus time after addition of 210 nM Fbxw7 TAMRA/Skp1 to 70 nM Cul1 NTD CFP pre-incubated with 70 nM β-TrCP. A single exponential fit gave k_{off} of 5 x 10^{-5} s^{-1}. Error bars: range of values, n=2.

CAND1 increases off rate of Fbxw7/Skp1

It has been reported that Fbox/Skp1 and CAND1 antagonize each other's binding to Cul1/Rbx1 (Goldenberg et al., 2004; Siergiejuk et al., 2009). Despite several attempts, we failed to create a fluorescent assay that measured the binding of CAND1 to Cul1/Rbx1 (data not shown). Thus, to measure directly CAND1's affect on SCF assembly, we added two-fold excess CAND1 to a preformed SCF^{Fbxw7} complex displaying FRET. We observed a significantly reduced amount of FRET after five minutes, indicating that CAND1 interferes with Fbxw7/Skp1 binding to Cul1/Rbx1 (Figure 3.2a). To ensure that this observation was not an artifact of our FRET assay, we repeated this measurement but included a chase of unlabeled Fbox/Skp1 when we added CAND1. The FRET signal was further reduced to no FRET in the same five minute time span. Importantly, when we repeated these experiments with neddylated Cul1, CAND1's effect was eliminated (Figure 3.2b).

These observations are surprising for several reasons. First, the short time span used here is in direct contrast to the slow off rate observed in Figure 3.1e indicating that CAND1 is not acting as a competitive inhibitor that must wait for Fbxw7/Skp1 to dissociate. Second, this implies that CAND1 is an allosteric regulator

of SCF complexes that actively remodels them in the absence of any energy input such as ATP. Third, given that CAND1 has two major binding sites on the N-terminus (NTD) and the C-terminus (CTD) of Cul1, these results suggest that disruption of CAND1's CTD binding site by the Nedd8-induced conformational change dramatically affects its ability to regulate Fbxw7/Skp1 binding at Cul1's NTD (Goldenberg et al., 2004; Duda et al., 2008). This is especially intriguing given that the NTD of Cul1 when bound to CAND1 or Fbox/Skp1 is nearly structurally identical.

To determine the mechanistic basis of CAND1's ability to remodel SCF complexes we measured the loss of FRET in real time upon addition of CAND1 to a preformed complex in a stop flow apparatus (Figure 3.2c). This loss of FRET fit well to a single exponential curve. Titration of CAND1 in this assay revealed increasingly rapid rates of SCF complex dissociation that followed saturation kinetics with a maximum rate of 1.3 s^{-1} and a half maximal concentration (K_m) of 26 nM (Figure 3.2d). To eliminate interference in our signal from re-association of Fbxw7/Skp1 to Cul1/Rbx1, we repeated our measurements with Fbox/Skp1 chase in the reaction (Figure 3.2d). The maximal rate of CAND1 dependent dissociation remained unchanged while the K_m increased to 53 nM (Figure 3.2d). In agreement with previous results, SCF complexes formed with neddylated Cul1 showed no dissociation in response to CAND1 in this assay (Figure 3.2d). However, when the assay was repeated on longer timescales, CAND1 had a modest 45-fold effect on the dissociation rate if Cul1 is neddylated (Figure 3.2e).

Three main points arise from this analysis. First, the saturation kinetics seen in this assay reveal the existence of a transient complex that contains CAND1,

Cul1/Rbx1, and Fbxw7/Skp1. Second, the K_m of 53 nM sets an upper limit on the Kd between CAND1 and Cul1/Rbx1 in the presence of Fbxw7/Skp1. Third, the maximal observed rate of 1.3 s^{-1} represents the rate of Fbxw7/Skp1 dissociation from the transient complex containing CAND1. The difference between the off rate of Fbxw7/Skp1 from Cul1/Rbx1 with and with out CAND1 is extraordinary. CAND1 actively changes the dissociation rate of SCF^{Fbxw7} a million-fold. Neddylation of Cul1 nearly abolishes the effect of CAND1, decreasing the dissociation rate of SCF^{Fbxw7} 30,000 fold in the presence of CAND1.

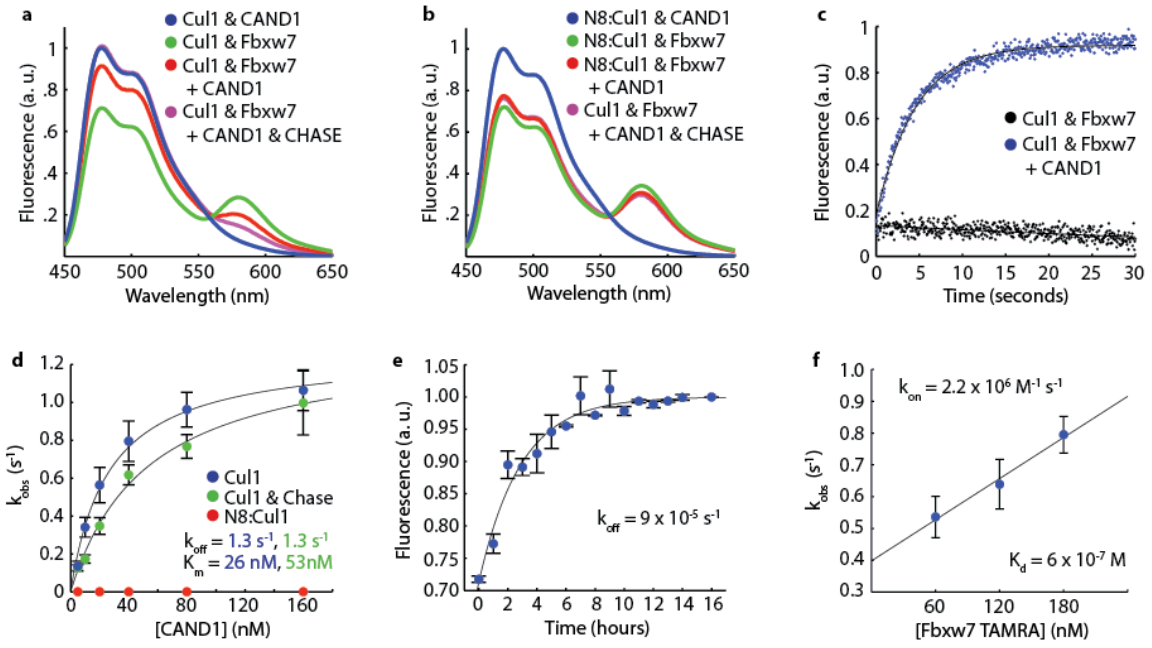

Figure 3.2 | CAND1 Actively Removes Fbxw7/Skp1 By Altering Off Rate. a, As in Figure 3.1a and Figure 3.1d except with the addition of 150 nM CAND1. **b,** As in a, except using neddylated Cul1 NTD CFP. **c,** The change in donor fluorescence versus time in a stop flow apparatus upon addition of 150 nM CAND1 with 50 nM Cul1 NTD CFP/Rbx1 pre-incubated with 50 nM Fbxw7 TAMRA/Skp1. **d,** The single exponential observed rates for various CAND1 concentrations mixed with 5 nM Cul1 NTD CFP/Rbx1 or 5nM neddylated Cul1 NTD CFP/Rbx1 pre-incubated with 5 nM Fbxw7 TAMRA/Skp1. Chase indicates 700 nM Skp2/Skp1. Error bars: +/- SD, n≥3. **e,** As in Figure 3.1e except with 150 nM

CAND1 and 700 nM Skp2/Skp1 chase mixed with 70nM neddylated Cul1 NTD CFP pre-incubated with 70 nM Fbxw7 TAMRA/Skp1. Error bars: range of values, n=2. **f,** As in Figure 3.1c, except with 150 nM CAND1 pre-incubated with 5 nM Cul1 NTD CFP/Rbx1. Error bars: +/- SD, n≥3.

CAND1 only affects SCF dissociation

The above data are consistent with previous observations that lead to the conclusion that CAND1 functions as a neddylation dependent inhibitor of SCF complex formation. Yet, the dramatic increase in off-rate measured above is not itself proof that CAND1 is an inhibitor. To determine directly if CAND1 is an inhibitor, we measured the association rate of Fbxw7 TAMRA/Skp1 and Cul1 NTD CFP/Rbx1 pre-incubated with a saturating concentration of CAND1. Shockingly, CAND1 did not affect the association rate of SCF^{Fbxw7} (Figure 3.2f). To better understand how CAND1 specifically modulates the dissociation rate of SCF complexes and not the associate rate we took advantage of the observation that CAND1 inhibits neddylation of Cul1/Rbx1 *in vitro*, and that this inhibition is relieved by Fbox/Skp1 complexes (Siergiejuk et al., 2009). We designed an assay using radiolabeled Cul1 to follow neddylation in real time. Near stoichiometric amounts of CAND1 inhibited neddylation of Cul1. Three different Fbox/Skp1 complexes suppressed CAND1's ability to inhibit neddylation in a manner dependent on acidic loops in Skp1 that are unnecessary for ubiquitylation (Figure 3.3a & Supplementary Figure B.1f).

Three major points emerge from these experiments. First, CAND1 does not act as a classic inhibitor of SCF complexes because CAND1 does not block

Fbox/Skp1 complexes from binding to Cul1/Rbx1. Second, Fbox/Skp1 complexes have the ability to remove CAND1 in a manner that is dependent on the acidic loops in Skp1. Third, these results suggest why CAND1 does not sequester Cul1/Rbx1 *in vivo* when neddylation is inhibited (Bennett et al., 2010). Although neddylation allows for extremely tight binding in the presence of CAND1, in the absence of neddylation SCF complexes still have a K_d of 600 nM.

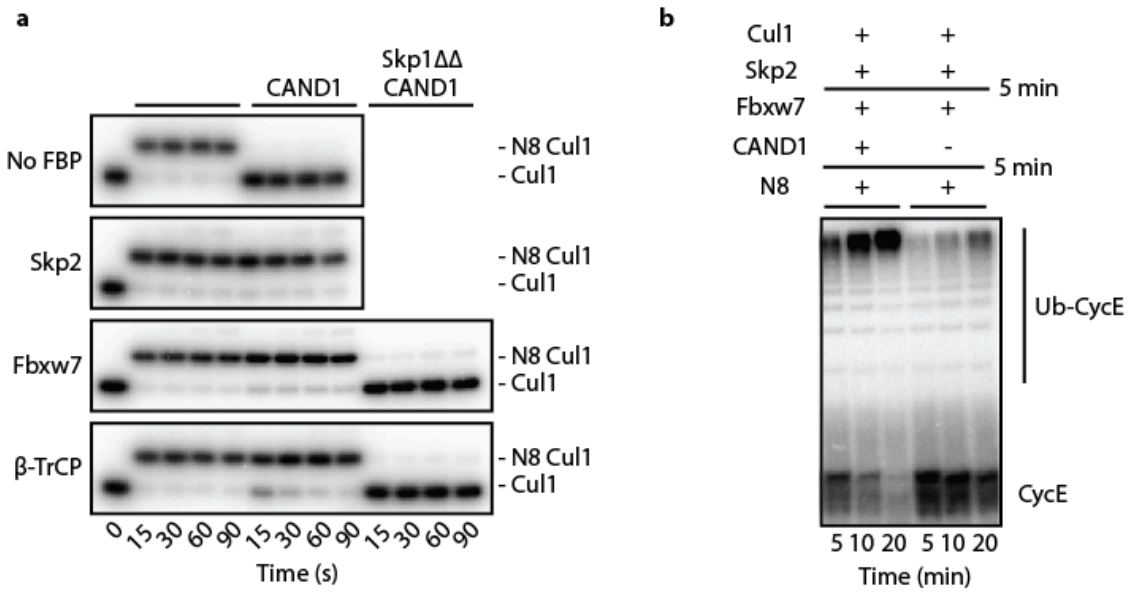

Figure 3.3 | Fboxes Remove CAND1. a, 100 nM radiolabeled Cul1/Rbx1 PKA preincubated with 300 nM CAND1 was mixed with pre-incubated 15 μM Nedd8, 300 nM Fboxes/Skp1, 1 μM Nedd8 E1, and 10 μM Ubc12. **b,** 150 nM Cul1/Rbx1 was pre-incubated with 150 nM Skp2/Skp1 for 5 min then mixed with 150 nM Fbxw7/Skp1, 600 nM radiolabeled CycE and either buffer or 200 nM CAND1. After 5 min, 15 μM Nedd8, 1 μM Nedd8 E1, and 10 μM Ubc12 were added to the mix. After 5 min, pre-incubated 60 μM Ubiquitin, 1 μM Ubiquitin E1, and 10 μM Cdc34b were added to the mix.

CAND1 functions as an Fbox exchange factor

Inspection of Figure 3.4, which summarizes all the rates measured here, suggests a manner in which CAND1 can stimulate activity in a purified system. If multiple Fboxes are used in the same ubiquitylation assay, then pre-incubation with saturating amounts of Fbox/Skp1 relative to Cul1/Rbx1 should reduce the rate of ubiquitylation of a second Fbox/Skp1. However, addition of CAND1 should allow the second Fbox/Skp1 complex access to Cul1/Rbx1. Neddylation of the complexes should then lock them down in respect to CAND1. Under these conditions, CAND1 did in fact stimulate the ubiquitylation assay (Figure 3.3b). Taken together, CAND1 appears to function as an exchange factor that drastically modulates the direct assembly of SCF complexes in a neddylation dependent manner.

Here we establish the first kinetic framework for the dynamic assembly of SCF complexes using a direct real time biophysical assay. We conclude that CAND1 is directly involved in the assembly of SCF complexes because it serves as an exchange factor for Fbox/Skp1 complexes. Our kinetic framework serves as a starting point to re-evaluate the function of CAND1 *in vivo*. Three ideas emerge from the synthesis of our kinetic model and genetic studies. First, CAND1 may be necessary for incorporation of newly synthesized Fboxes if all the Cul1/Rbx1 complexes are saturated. Second, CAND1 may be needed to release ubiquitylated Fboxes from Cul1/Rbx1 to ensure their proper degradation. Third, CAND1 may function as an exchange factor that is specifically localized, giving another layer of control over SCF complex assembly in the cell.

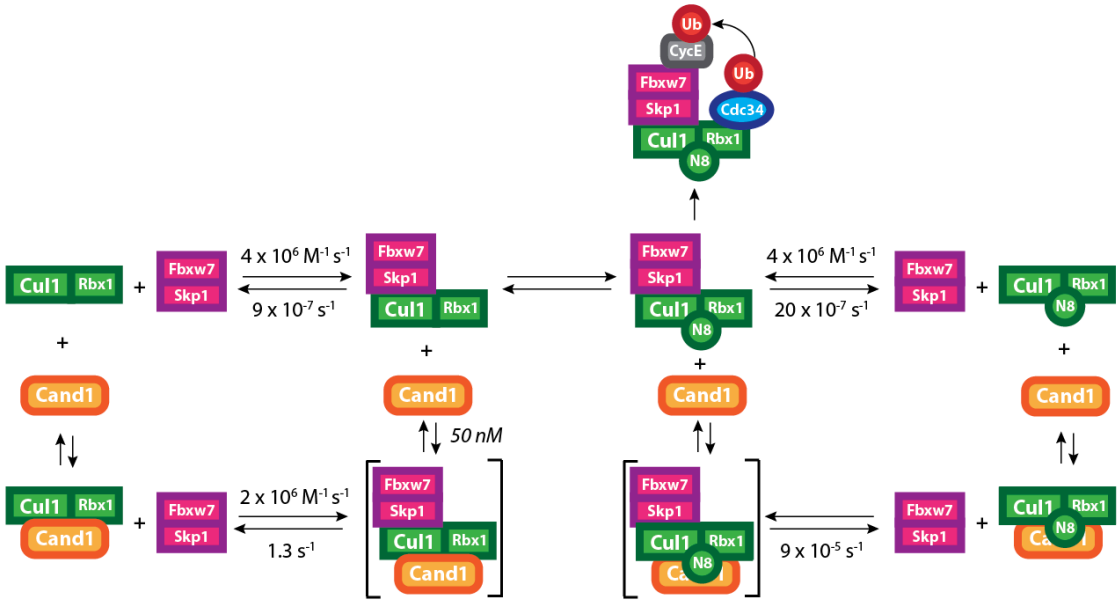

Figure 3.4 | Fboxes Remove CAND1. The model is derived from all the rates measured here. The transient complex is in brackets.

Methods

Fluorimeter scans were performed on FluoroLog-3 (Jobin Yvon) in a buffer containing 30 mM Tris pH 7.6, 100 mM NaCl, 0.5 mM DTT, and 1 mg/ml Ovalbumin (Sigma) in a volume of 250 µl. Mixtures were excited at 430 nm and the emissions were scanned from 450 nm to 650 nm. Stop flow reactions were performed on a Kintek stop flow machine in the same buffer as the fluorimeter scans. Ubiquitylation reactions were performed as described (Pierce et al., 2009). Proteins were purified as described (Pierce et al., 2009).

Chapter 4:

Unpublished Work

This chapter is included to provide a summary of the many assays and experiments that were not taken to completion. Most, but not all, of the experiments that have found their way into this chapter provide evidence for a conformational change in SCF upon substrate binding. Likely, this change is occurring in the Fbox protein and is independent of neddylation status. However, there are several contradictory results, and the function of this conformational change, if it does exist, remains a mystery. It is my hope that including this chapter here will stimulate further work on this topic.

Substrate Induced Conformational Change

The ubiquitylation rates for human SCF complexes show a clear inconsistency between the multi-turnover k_{cat} and the observed single turnover rate (Saha and Deshaies, 2008). For $SCF^{\beta\text{-}TrCP}$ and Cdc34, the k_{cat} is 0.05 min^{-1} and the k_{obs} for single turnover is 0.3 min^{-1}. For neddylated $SCF^{\beta\text{-}TrCP}$ and Cdc34, the k_{cat} is 0.2 min^{-1} and the k_{obs} for single turnover is 3 min^{-1}. When starting with a mono-ubiquitylated substrate, the k_{cat} is 2 min^{-1} and the k_{obs} for single turnover is >20 min^{-1}. Under all conditions tested, the single turnover rate is faster than the multi-turnover, indicating that a step after the transfer of ubiquitin is rate-limiting. Currently, the origin of this phenomenon remains unclear.

Previously, a yeast single encounter ubiquitylation revealed that the rate-limiting first ubiquitin transfer for SCF^{Cdc4} and its substrate CycE is 0.2 s^{-1} and the off rate of CycE and its ubiquitylated products is 0.4 s^{-1} (Pierce et al., 2009). To determine if the above phenomenon seen for human SCF complexes also occurs in

yeast SCF complexes, I adapted the yeast ubiquitylation assay previously used for single encounter reactions to multi-turnover reactions (Pierce et al., 2009). At a saturating concentration of CycE, the multi-turnover rate for ubiquitylation was 0.03 s^{-1} (Figure 4.1). Importantly, the positive intercept for the multi-turnover reaction in Figure 4.1 indicates that a burst phase was present in this reaction. When I repeated the reaction on a quench flow apparatus for higher time resolution and with a lower concentration of substrate, a clear burst phase emerged (Figure 4.2). The rate constant of the first phase in Figure 4.2 is 0.24 s^{-1}, in good agreement with the rate-limiting first ubiquitin transfer. The second phase has a rate constant of 0.03 s^{-1}, consistent with the multi-turnover rate constant seen with saturating substrate. However, these numbers present a conundrum. The off rate of product and substrate (0.4 s^{-1}) is faster than the rate observed here (0.03 s^{-1}) indicating that a step after dissociation and before ubiquitin transfer is rate-limiting for the full enzymatic cycle. Yet, the association of CycE and SCF^{Cdc4} cannot be rate-limiting given that we observe the same rate when we have saturating concentrations of CycE (Figure 4.1). This indicates that a step between substrate association and ubiquitin transfer is rate-limiting. How then is it possible to see a burst phase? The reaction set up used here was to pre-incubate CycE with SCF^{Cdc4} before the reaction. Thus, it was possible for any rate-limiting step after association but before transfer to be bypassed at the start of the reaction. This predicted that a lag phase should occur if CycE and SCF^{Cdc4} were not pre-incubated at the beginning of the reaction. Indeed, in a single turnover reaction, using wild type ubiquitin, a lag phase that contains a rate of 0.024 s^{-1} was observed (Figure 4.3) (Pierce et al., 2009). An

accurate measurement of the association rate of CycE and SCF^{Cdc4}, however, has not been made. In order to reconcile all of the measured rates, I insert an extra step in between substrate association and ubiquitin transfer (Figure 4.4). Likely, this represents a conformational change induced by the substrate in SCF^{Cdc4}. My sole attempt to measure this rate directly, was to fluorescently label the only lysine in CycE and the active site of Cdc34, which is the only cysteine in the protein. I knew that the lysine in CycE and the cysteine in Cdc34 had to come close to each other for the first ubiquitin transfer. Thus, I hypothesized that they would FRET. This FRET signal would likely occur after the rate limiting conformational change, if it existed, given that it occurred before the ubiquitin transfer. There was a small amount of FRET seen when Cdc34, SCF^{Cdc4}, and CycE were all mixed together, however, there were also numerous anomalies from several control mixing experiments (Figure 4.5). Despite this I attempted to measure rates directly in the stop flow. The result was a three phase curve (Figure 4.6). The first phase was a noisy fast single exponential with an observed rate of 1.8 s^{-1} that likely represents CycE associating with SCF^{Cdc4} and a low FRET state (i.e. CycE is close enough to Cdc34 to FRET but it is not efficient). Then comes a lag phase curve in which the two phases fit to exactly the same rate, 0.017 s^{-1}. This high FRET state likely represents CycE moving closer to the active site of Cdc34. The rates seen here are in agreement with the slow rate measured in all other assays. However, the reason for a lag phase with identical rates is unclear. Unfortunately, many of the measurements made here were not repeated nor assays optimized because I moved to using the human system as a direct result of comments from reviewers of the Pierce et al., 2009.

When I repeated multi-turnover experiments with human $SCF^{\beta\text{-}TrCP}$ and SCF^{Fbxw7} no burst phase was seen and both complexes displayed rates of 0.18 min^{-1} (Figure 4.7). This matches the single turnover rate seen in Saha and Deshaies, 2008. However, these reactions were performed with Fboxes that had been purified with Skp1ΔΔ. When this was repeated with SCF^{Fbxw7} with full length Skp1 and with Skp1ΔΔ, the reactions were the same with no burst phase evident (Figure 4.8). Thus, the dynamics seen with the yeast system did not match the dynamics seen with the subsequent human system. It is unclear at this time why Saha and Deshaies, 2008 had a difference in multi-turnover versus single turnover rates, however, I suspect that in the multi-turnover reactions, substrate was not saturating. The reason for the burst phase kinetics seen in the yeast system may be explainable by the observation that the attachment of the Nedd8 homologue Rub1 to Cdc53 does not increase the rate ubiquitin transfer for SCF^{Cdc4} (Pierce et al., 2009). Given that Rub1 is not essential in this organism in direct contrast to Nedd8 in all other organisms, the yeast system may have evolved a mechanism for inducing the active conformation of Cdc53/Rbx1 without Rub1.

The processive measurements performed in Pierce et al., 2009 did not include SCF^{Fbxw7}. I performed reactions similar to Figure 2.1a (Pierce et al., 2009) with both naked and neddylated Cul1 using either Cdc34 or UbcH5 (Figure 4.9). These reactions were fractionated on large gradient gels. As with $SCF^{\beta\text{-}TrCP}$, the length of chain was quite long in a single encounter (~15 ubiquitins) when using Cdc34. The speed of the reaction was stimulated and the processivity increased by neddylation. UbcH5 reactions on the other hand, were not very processive,

containing mainly mono-ubiquitylated species in a single encounter. The reactions in this case were not stimulated much by neddylation.

To investigate changes in the neddylation rate of human SCF complexes based on their composition, I performed steady state measurements with and without Fbxw7/Skp1 and its substrate CycE (Figure 4.10). The rates measured for with and without Fbxw7/Skp1 was the same (0.7 s^{-1}). However, there was a distinct lag phase when CycE was included in this reaction. The reason for this observation remains unclear.

Lastly, the original reason for the developing the fluorescent Fboxes was to measure the dynamics of substrate binding. Using a CycE substrate synthesized with a KFAM derivative instead of a PKA site and a Fbxw7 labeled with AMC through a sortase reaction, I was able to observe a small amount of FRET that could be chased away with unlabeled CycE (Figure 4.11). The reaction was not optimized and should be noted that the Fbxw7 AMC/Skp1 did show bleaching that was significant relative to the signal change (Figure 4.11a). However, the off rate measured in the stop flow using this assay was 0.2 s^{-1}, which is in excellent agreement with the quench flow assays done with SCF^{Cdc4} and $SCF^{\beta\text{-}TrCP}$ in Pierce et al., 2009 (Figure 4.12, yellow curve). The on-rate measurements, however, were confounded by a significant bleaching component. However, the rate of the reaction clearly increased with increasing CycE KFAM acceptor. Importantly, when Fbxw7 AMC/Skp1 was pre-incubated with non-labeled CycE, this association reaction was stimulated (Figure 4.12, compare the magenta line with the black line). This behavior was predicted by

the model in Figure 4.4, yet is unclear at this time why there does not exist biphasic behavior in multi-turnover ubiquitylation reactions with SCF^{Fbxw7}.

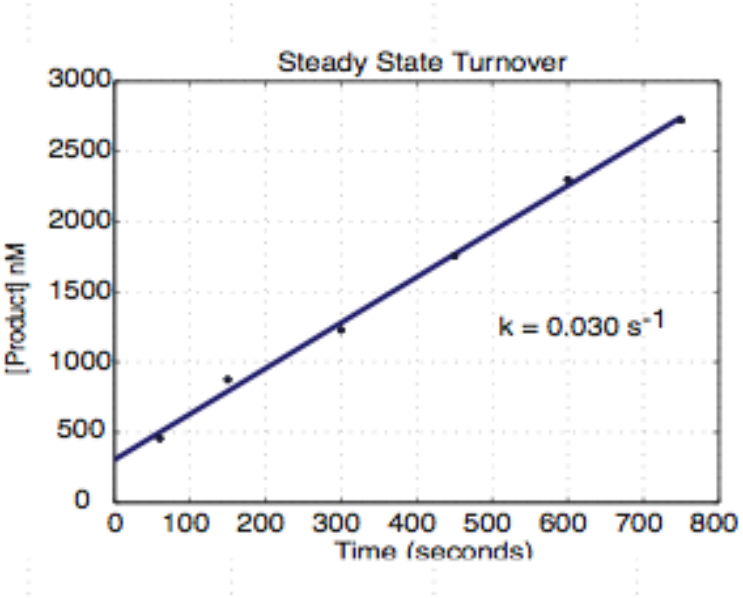

Figure 4.1 | Steady State Reaction of yeast SCF^{Cdc4} at Saturating Substrate. 10 μM radiolabeled CycE was pre-incubated with 150 nM SCF^{Cdc4} and mixed with 15 μM K0 ubiquitin pre-incubated with 10 μM Cdc34 and 1 μM Uba1.

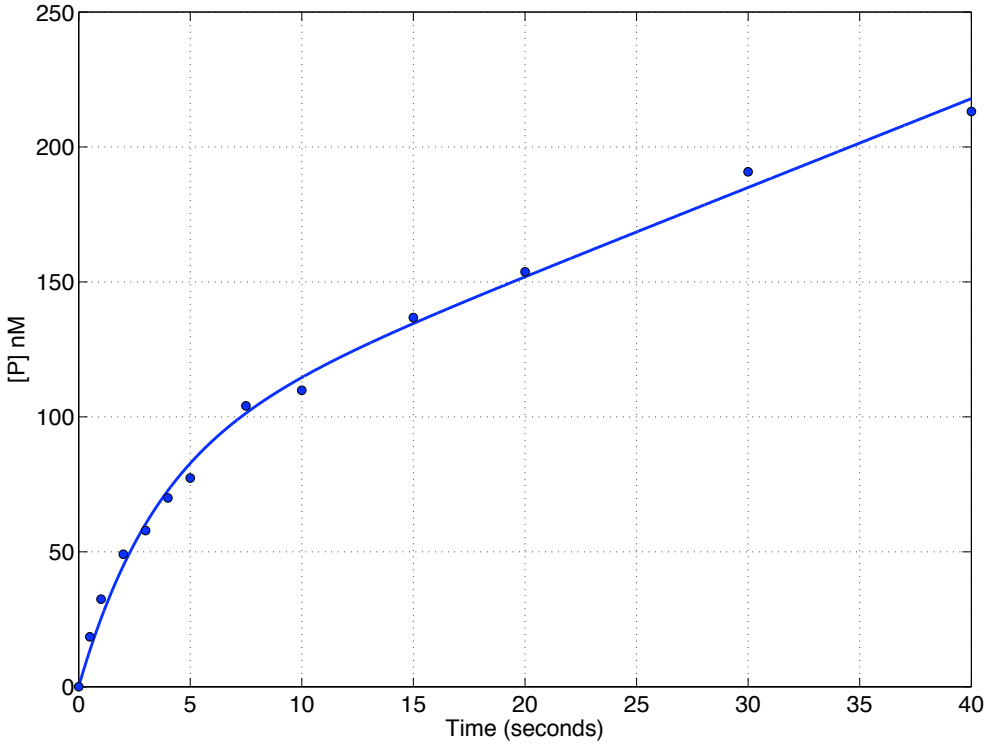

Figure 4.2 | Burst Phase of SCF^{Cdc4} Multi-turnover Reaction. 600 nM radiolabeled CycE was pre-incubated with 150 nM SCF^{Cdc4} and mixed with 15 μM K0 ubiquitin pre-incubated with 10 μM Cdc34 and 1 μM Uba1. The amplitude of the burst is 120 nM, the faster first phase has a rate of 0.24 s^{-1}, and the slower linear phase has a rate of 0.03 s^{-1}.

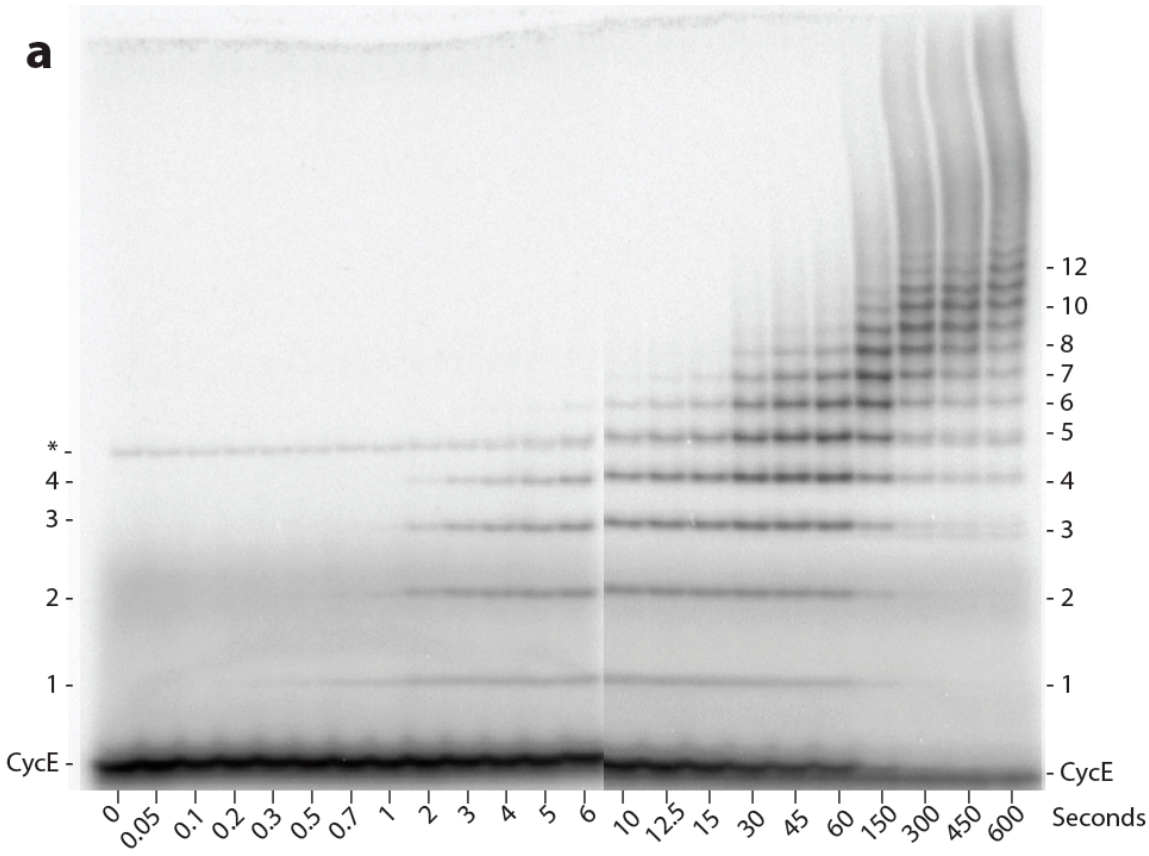

Figure 4.3 | A Lag Phase Exists If CycE and SCF^{Cdc4} Are Not Pre-incubated. This is the raw data from Figure 2.2c (Pierce et al., 2009). A clear lag phase can be seen.

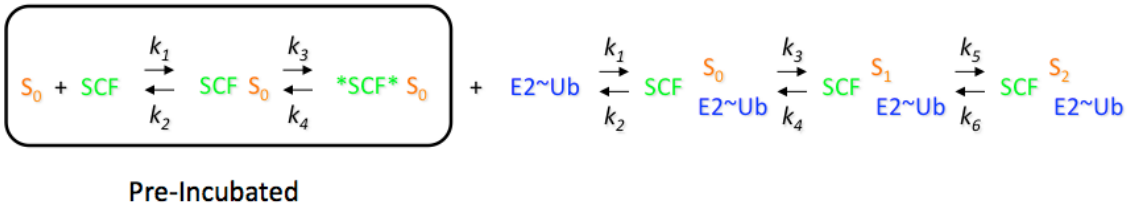

Figure 4.4 | Model with conformational change inserted. Inserting a step in between substrate binding and ubiquitin transfer that can occur during SCF^{Cdc4} and CycE pre-incubation allows for a simple model that explains the dynamics seen.

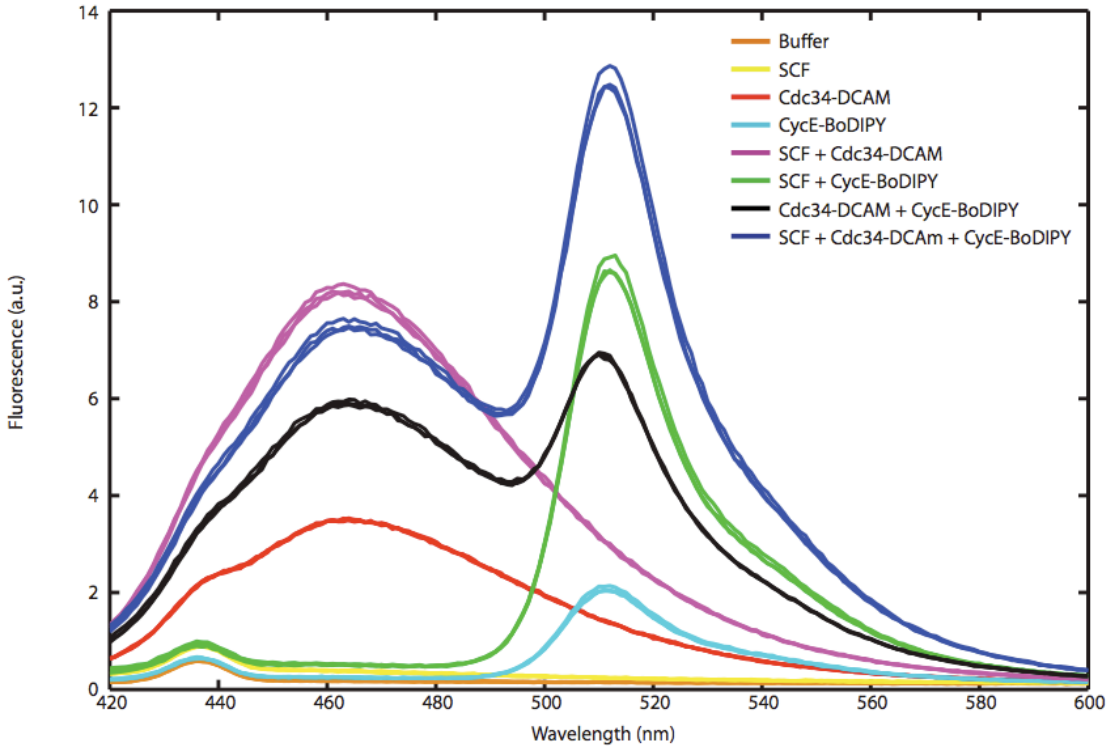

Figure 4.5 | Attempted FRET Measurements for CycE and Cdc34. 200 nM CycE reacted with BODIPY Fluorescein Succinimidyl Ester and 40 nM Cdc34 reacted with DACM, N-(7-dimethylamino-4-methylcoumarin-3-yl) maleimide were mixed in several combinations with 100 nM SCF^{Cdc4}. Scans are excited at 380 nm with emission from 420 nm to 600 nm.

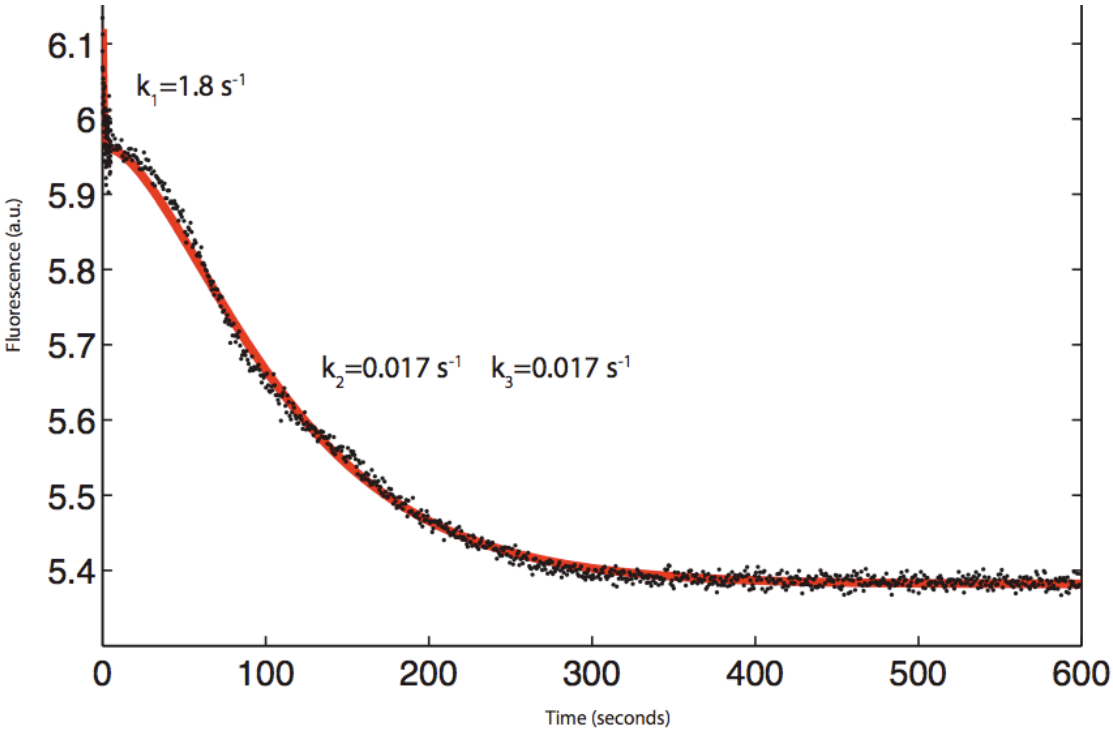

Figure 4.6 | Association of CycE and Cdc34 in a stop flow. The reaction in Figure 4.5 performed on the stop apparatus with a filter to follow only the donor signal. Three phases are evident.

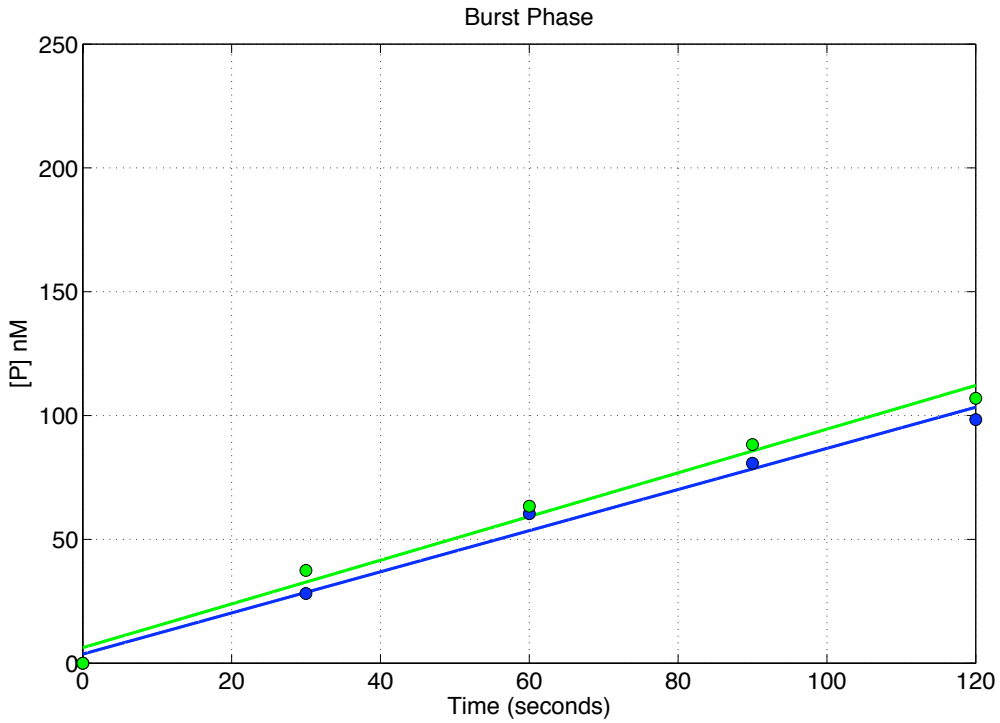

Figure 4.7 | $SCF^{\beta\text{-}TrCP}$ and SCF^{Fbxw7} have no burst phase. 600 nM radiolebed substrate (either CycE or β-cat) was pre-incubated with 150 nM SCF complexes and reacted with 10 μM Cdc34b. $SCF^{\beta\text{-}TrCP}$ and SCF^{Fbxw7} have rates of 0.003 per second or 0.18 per min. This matches the single turnover rates Saha and Deahies, 2009 reported.

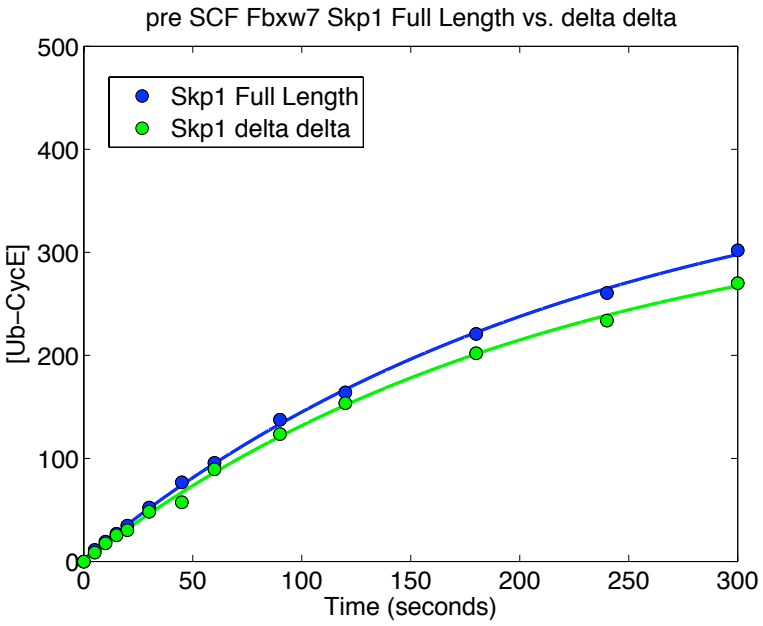

Figure 4.8 | SCF^{Fbxw7} with Skp1 full length or Skp1ΔΔ. Reaction conditions are the same as in Figure 4.7. When fit to exponentials or the initial points to a linear line, full length Skp1 in blue has rates of 0.012 per second and Skp1**ΔΔ** in green is 0.011 per second.

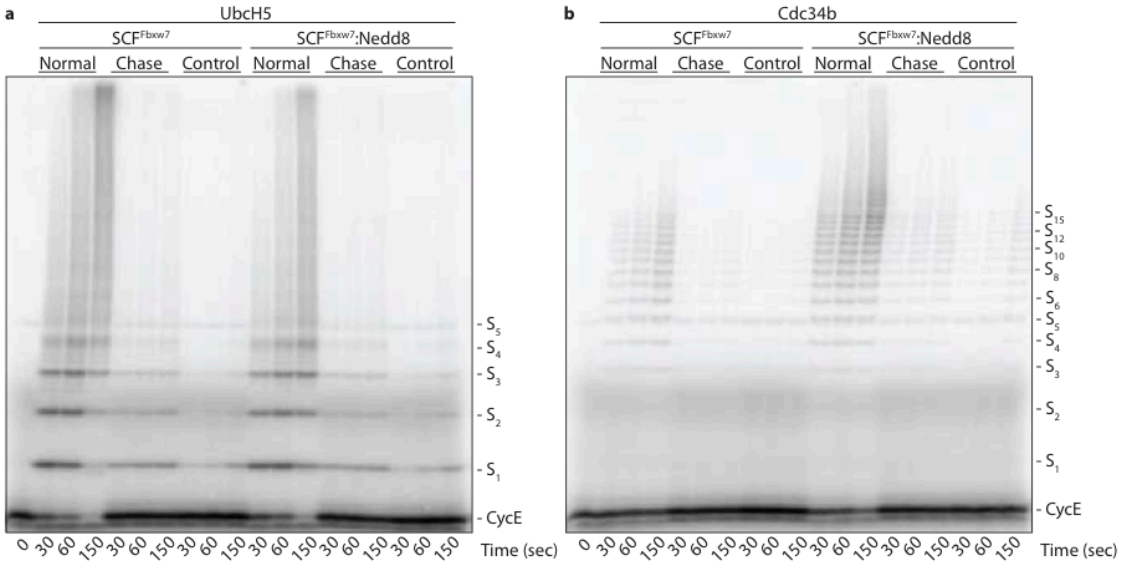

Figure 4.9 | Processivity of SCF^{Fbxw7} with Cdc34 and UbcH5. 10 nM radiolabeled CycE was pre-incubated with 150 nM SCF^{Fbxw7} that contained neddylated Cul1 as indicated. Either 10 μM of Cdc34b or UbcH5 were used.

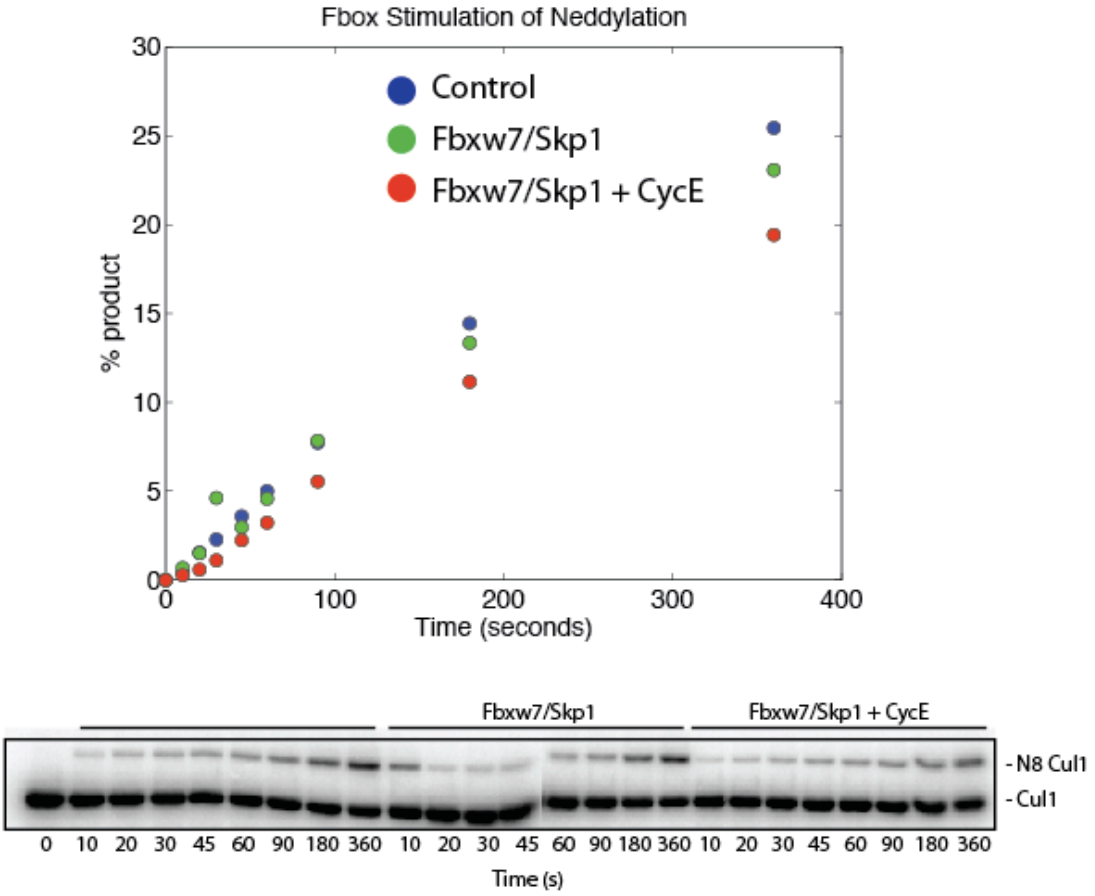

Figure 4.10 | Substrate and Fbox Affect Neddylation. Both have a rate of 0.7 per second, however, in the presence of substrate, there is a lag phase. 25 nM Nedd8 E1, 100 nM Ubc12, 6 μM Nedd8, 1 μM radiolabeled Cul1 PKA, 500 nM Fbxw7/Skp1, and 8 μM CycE.

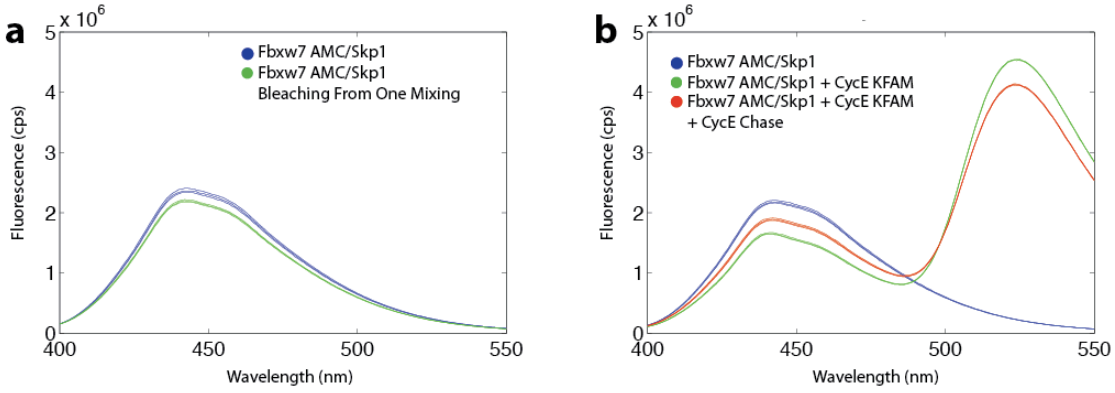

Figure 4.11 | FRET Between Fbxw7 AMC/Skp1 and CycE KFAM. a, Fluorimeter scans exciting at 380 nm and scanning from 400 to 550 nm. 30 nM Fbxw7 AMC in blue, then mixed to see extent of bleaching. **b,** 30 nM Fbxw7 AMC mixed with 580 nM CycE KFAM then 32 μM CycE as chase.

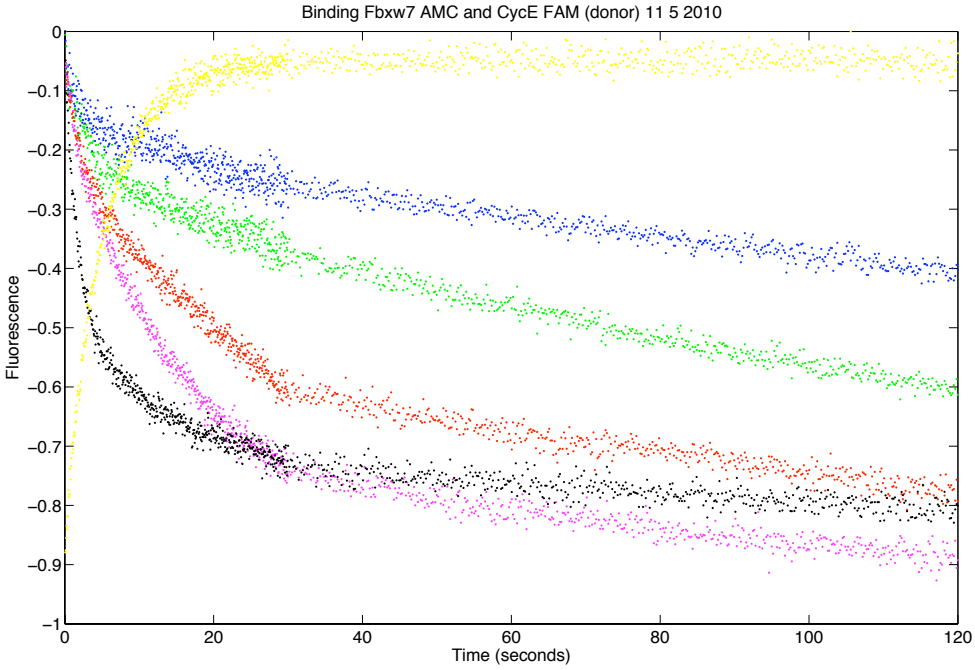

Figure 4.12 | Binding of CycE and Fbxw7 using FRET. 30 nM Fbxw7 AMC/Skp1 mixed with: Blue = 400 nM CycE KFAM, Green = 800 nM CycE KFAM, Red = 1.6 μM CycE KFAM, Magenta = 3.2 μM CycE KFAM, Black is 130 nM CycE pre-incubated 30 nM Fbxw7 AMC then mixed with 3.2 μM CycE KFAM. Yellow is starting with 3.2 μM CycE KFAM and mixing with excess CycE as a chase gives an off rate of 0.2 per second. Note that the machine was set for two phase time courses with the first phase from 0 to 30 seconds (collect 500 time points) and the second phase from 30 seconds to 120 seconds (collect 500 time points). Clearly this had an effect on the data, which I attributed to bleaching and low FRET signal.

Appendix A: Supplementary Materials for Chapter 2

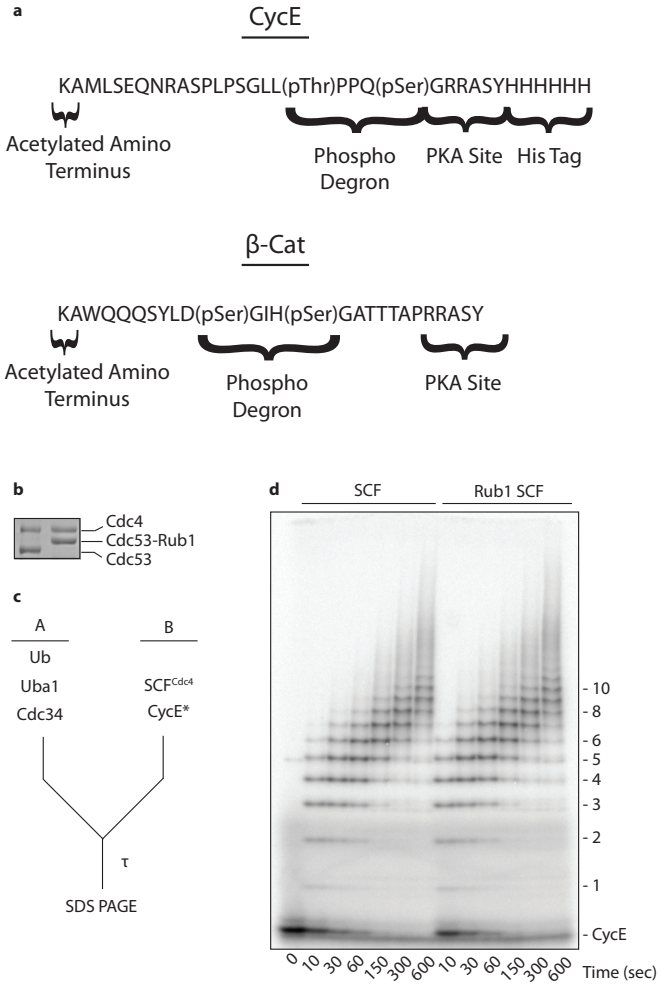

Supplementary Figure 1 | Attachment of Rub1 to SCFCdc4 did not change ubiquitylation kinetics of CycE. **a,** The design of CycE and β-Cat. The sequence from Lys1 through pSer23 is derived directly from human cyclin E1. **b,** SCFCdc4 was bound to beads coupled to the anti-Py antibody. Beads were mixed with purified Rub1, Ula1–Uba3, Ubc12, and ATP. After washing, the Rub1-conjugated SCFCdc4 was released with the Py peptide and analyzed by SDS-PAGE followed by staining with Coomassie Blue. Lane 1: unmodified SCFCdc4, lane 2: Rub1-conjugated SCFCdc4. **c,** Reaction design: SCFCdc4 or Rub1-conjugated SCFCdc4 (150 nM) was pre-mixed with 32P labeled CycE (10 nM) and combined with pre-mixed ubiquitin (60 μM), Uba1 (0.8 μM), Cdc34 (10 μM), and ATP. **d,** Reactions were evaluated by SDS-PAGE followed by phosphor-imaging.

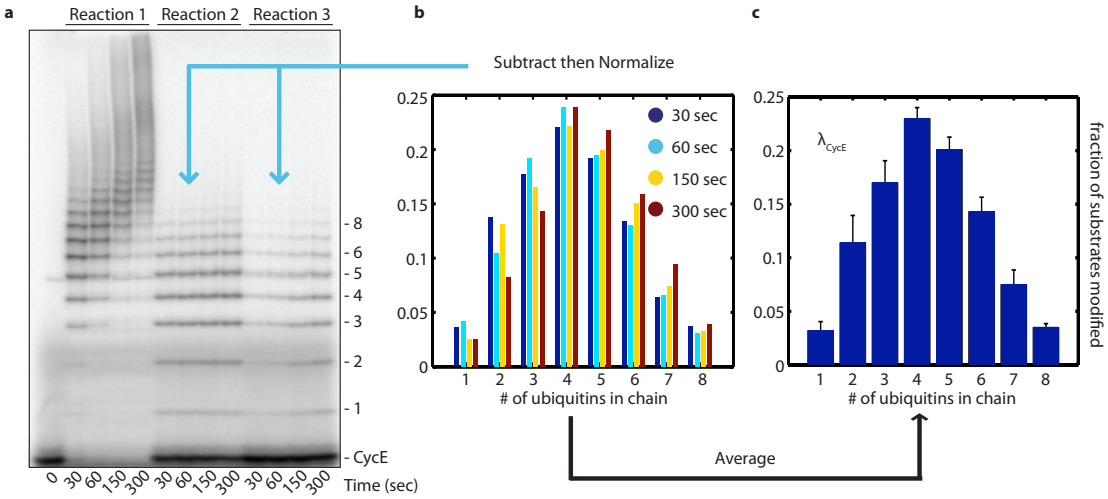

d

S_1	S_2	S_3	S_4	S_5	S_6	S_7	S_8
0.032	0.11	0.17	0.23	0.20	0.14	0.075	0.035
±0.0084	±0.026	±0.021	±0.010	±0.012	±0.014	±0.014	±0.0036

Normalized Average Final Distribution λ_{CycE}

e

S_1	S_2	S_3	S_4	S_5	S_6	S_7	S_8	S_9	S_{10}	S_{11}	S_{12}	S_{13}	S_{14}
0.04	0.05	0.07	0.11	0.11	0.13	0.13	0.11	0.09	0.07	0.04	0.02	0.01	0.01
±0.008	±0.008	±0.015	±0.015	±0.008	±0.01	±0.007	±0.013	±0.008	±0.012	±0.009	±0.006	±0.004	±0.005

Normalized Average Final Distribution $\lambda_{\beta\text{-cat}}$

f

K_d = 90 nM; $[SCF^{Cdc4}]$ = 150 nM; $[CycE_0]$ = 10 nM;

$[SCF{:}S_0] = 0.5 * (K_d + SCF + S_0) - [\,0.25 * (Kd + SCF + S_0)^2 - (SCF{*}S_0)\,]^{0.5}$

$[SCF{:}S_0]$ = 6.15 nM or 61.5% of S_0; On average 17% of S_0 is modified

17% / 61.5% = 27.6% of bound S_0 at the beginning of the reaction goes on to get modified

72.4% of bound S_0 at the beginning of the reaction does not get modified

g

K_d = 480 nM; $[SCF^{\beta\text{-}TrCP}]$ = 500 nM; $[\beta\text{-cat}_0]$ = 100 nM;

$[SCF{:}S_0] = 0.5 * (K_d + SCF + S_0) - [\,0.25 * (Kd + SCF + S_0)^2 - (SCF{*}S_0)\,]^{0.5}$

$[SCF{:}S_0]$ = 48.5 nM or 48.5% of S_0; On average 3.7% of S_0 is modified

3.7% / 48.5% = 7.6% of bound S_0 at the beginning of the reaction goes on to get modified

92.4% of bound S_0 at the beginning of the reaction does not get modified

Supplementary Figure 2 | Calculation of λ. a, For clarity, Figure 1a is reproduced here. **b,** The distributions of products in reaction 3 were subtracted from the distribution of products in reaction 2 at each time point and then normalized. **c,** The average of the distributions shown in b is λ_{CycE}. **d,** The fractional amounts of each product ($S_1 - S_8$) that comprise the distribution λ_{CycE}. **e,** The fractional amounts of each product ($S_1 - S_{14}$) that comprise the distribution $\lambda_{\beta\text{-Cat}}$. **f,** Calculation of the percent CycE bound to SCF^{Cdc4} at the beginning of the reaction, based on the reported K_d for binding of CycE to Cdc4.[21] Combined with the kinetics of Fig. 1a the percent of productive encounters was calculated. **g,** Calculation of the percent β-Cat bound to SCFβ-TrCP at the beginning of the reaction, based on the reported K_d for binding of Ub-β-Cat to β-TrCP.[22] Combined with the kinetics of Fig. 1b the percent of productive encounters was calculated.

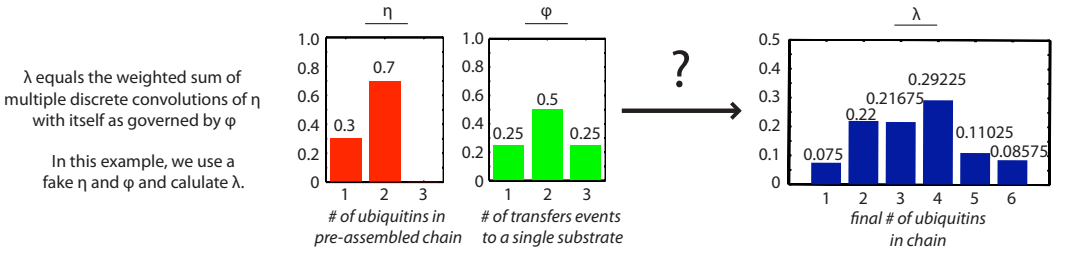

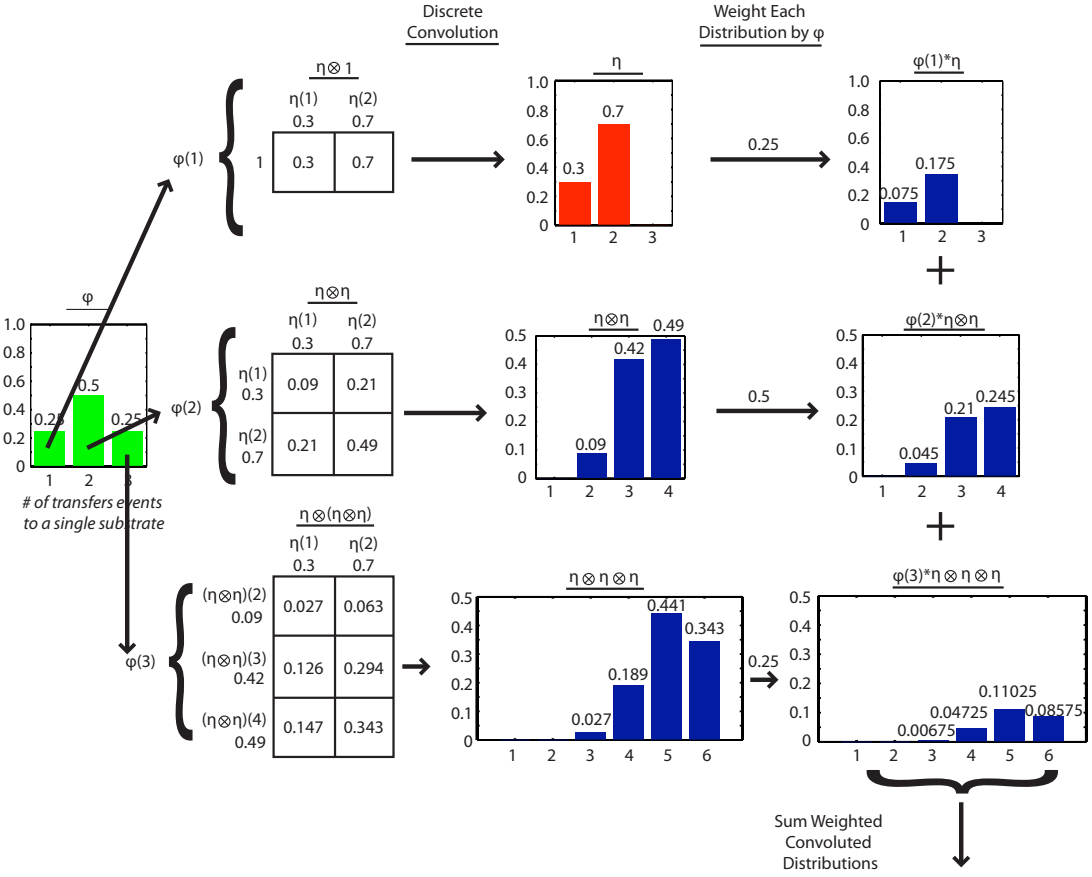

Supplementary Figure 3 | An example of calculating λ from η and φ. In this example, we assigned distributions to η and φ. To calculate λ, we took multiple convolutions of η with itself as governed by φ. In our example, 25% of substrates underwent one transfer, for which the η value determines that 30% were a single ubiquitin while 70% were diubiquitin. Thus, we weight the distribution η by the fraction of a single transfer, φ(1)*η. 50% of substrates underwent two transfers. Each of these two transfers selects from the pool of pre-assembled chains, thus we must consider the convolution of η with itself (ηη) and then w eight it by the fraction that receive two transfers, φ(2)*ηη. This process is repeated for the all indexes of φ, each time adding an additional convolution. These weighted distributions sum to give λ.

In this example, we use a fake η and λ and calulate φ .

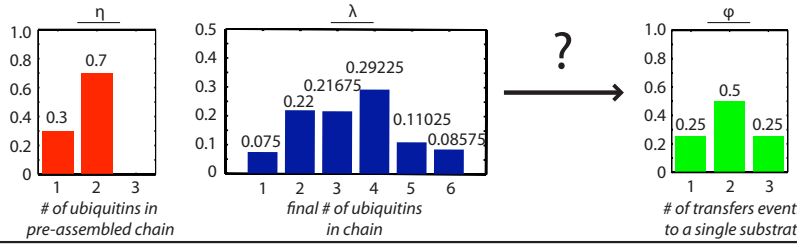

The only way to end up with 1 ubiquitin on substrate is from a single transfer of a single ubiquitin.

Thus, $\eta(1)*\varphi(1) = \lambda(1)$

$$\varphi(1) = \frac{\lambda(1)}{\eta(1)} = \frac{0.075}{0.3} = 0.25$$

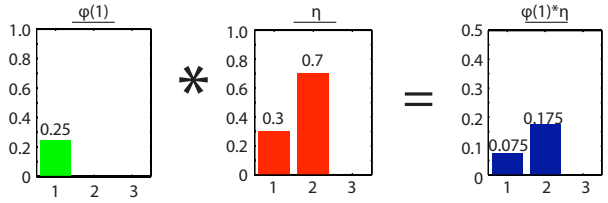

Subtract the contribution of φ(1) from λ

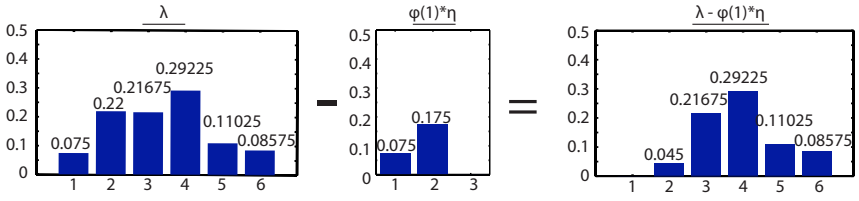

After substracting the contribution of single transfers, the only way to end up with 2 ubiquitins on substrate is from two transfers of a single ubiquitin.

Thus, $\eta(1)*\eta(1)*\varphi(2) = [\lambda - \varphi(1)*\eta](2)$

$$\varphi(2) = \frac{[\lambda - \varphi(1)*\eta](2)}{\eta(1)*\eta(1)} = \frac{0.045}{0.3*0.3} = 0.5$$

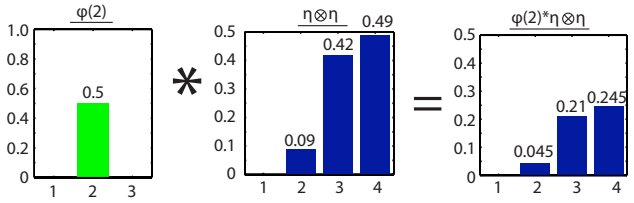

Subtract the contribution of φ(2) from λ already corrected for φ(1)

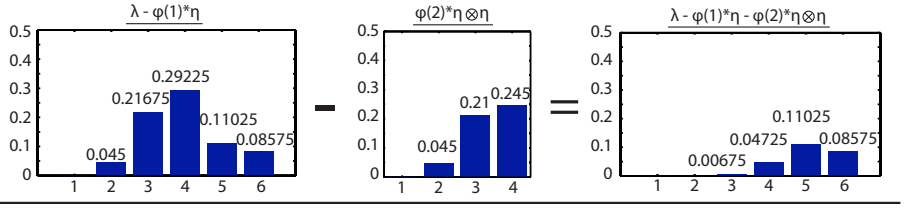

After substracting the contribution of single and double transfers, the only way to end up with 3 ubiquitins on substrate is from three transfers of a single ubiquitin.

Thus,

$\eta(1)*\eta(1)*\eta(1)*\varphi(3) = [\lambda - \varphi(1)*\eta - \varphi(2)*\eta\otimes\eta](3)$

$$\varphi(3) = \frac{[\lambda - \varphi(1)*\eta - \varphi(2)*\eta\otimes\eta](3)}{\eta(1)*\eta(1)*\eta(1)} = \frac{0.00675}{0.3*0.3*0.3} = 0.25$$

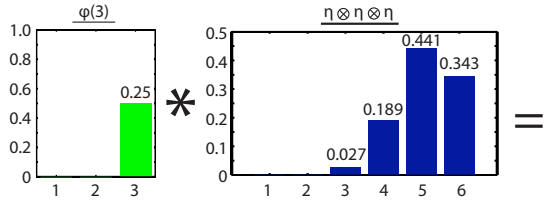

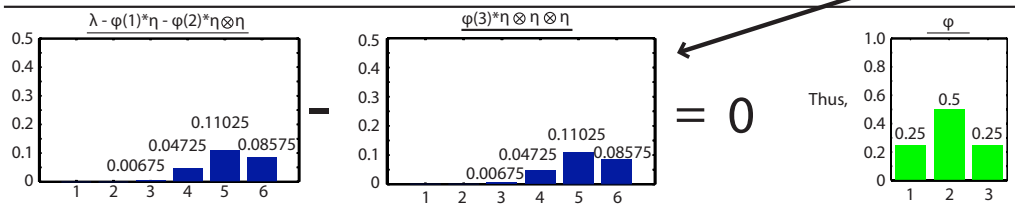

Supplementary Figure 4 | An example of calculating φ from λ and η. Deconvolution took advantage of the constraints existing on the lowest index of λ. Here we used λ and η from the example in Supplementary Figure 3. The only way of creating the species in λ that has a single ubiquitin attached to substrate was by the single transfer of a single ubiquitin. Thus, φ(1)*η(1) equals λ(1) and φ(1) is calculated by division. The contribution of φ(1) to λ was then calculated and subtracted from λ. The only way remaining to form λ(2), is by two transfers of a single ubiquitin. Thus φ(2) equals [λ-φ(1)*η](2)/[η(1)*η(1)]. This process is repeated until φ is revealed.

a

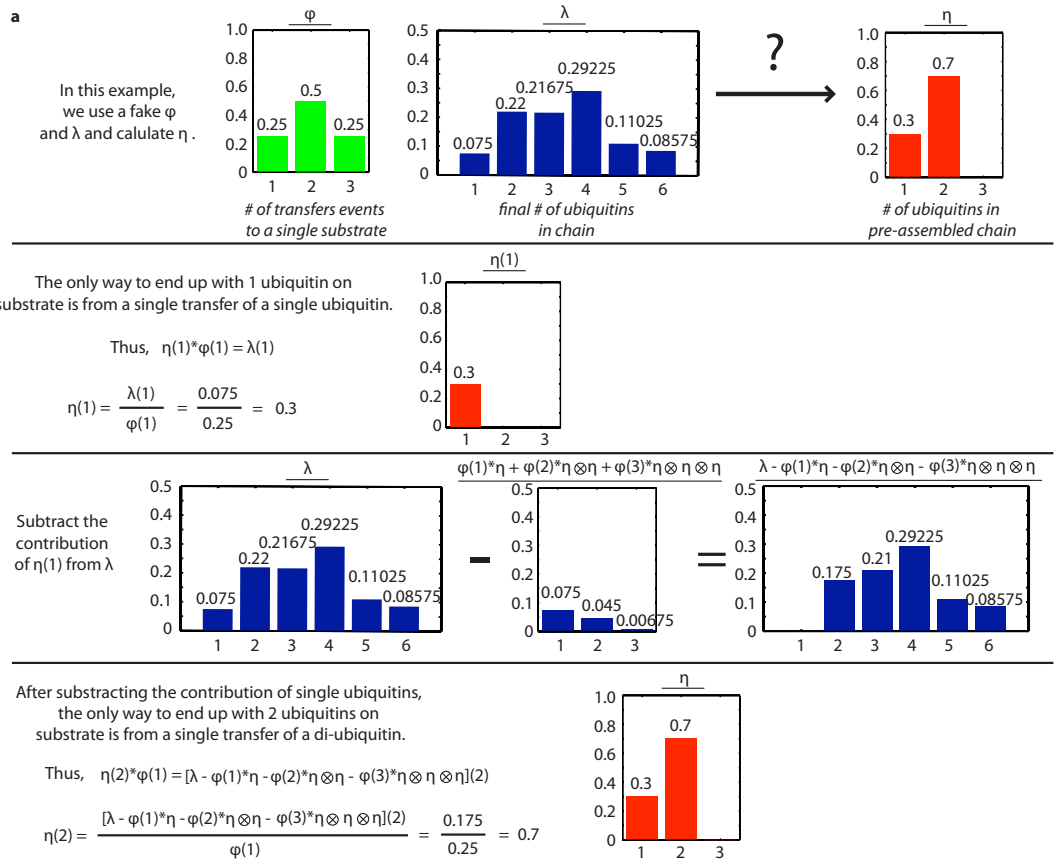

b

Exponential normalized distributions of η with varying rate parameter α $e^{-\alpha*\eta(i)}$

α	η(1)	η(2)	η(3)	η(4)	η(5)	η(6)	η(7)	η(8)	Sum(η)
0.1	1.0000	0.0000	0.0000	0.0000	0.0000	0.0000	0.0000	0.0000	1.0000
0.2	0.9933	0.0067	0.0000	0.0000	0.0000	0.0000	0.0000	0.0000	1.0000
0.3	0.9643	0.0344	0.0012	0.0000	0.0000	0.0000	0.0000	0.0000	1.0000
0.4	0.9179	0.0753	0.0062	0.0005	0.0000	0.0000	0.0000	0.0000	1.0000
0.5	0.8647	0.1170	0.0158	0.0021	0.0003	0.0000	0.0000	0.0000	1.0000
0.6	0.8111	0.1532	0.0289	0.0055	0.0010	0.0002	0.0000	0.0000	1.0000
0.7	0.7604	0.1822	0.0437	0.0105	0.0025	0.0006	0.0001	0.0000	1.0000
0.8	0.7135	0.2044	0.0586	0.0168	0.0048	0.0014	0.0004	0.0001	1.0000
0.9	0.6709	0.2209	0.0727	0.0239	0.0079	0.0026	0.0009	0.0003	1.0000
1.0	0.6323	0.2326	0.0856	0.0315	0.0116	0.0043	0.0016	0.0006	1.0000

φ as given by the muliptle weighted sums deconvolution of exponential η (above) and λ

α	φ(1)	φ(2)	φ(3)	φ(4)	φ(5)	φ(6)	φ(7)	φ(8)	Sum(φ)
0.1	0.0320	0.1140	0.1700	0.2300	0.2010	0.1430	0.0750	0.0350	1.0000
0.2	0.0322	0.1153	0.1719	0.2328	0.2015	0.1420	0.0727	0.0334	1.0018
0.3	0.0332	0.1214	0.1805	0.2454	0.2032	0.1368	0.0619	0.0265	1.0089
0.4	0.0349	0.1322	0.1959	0.2682	0.2027	0.1255	0.0409	0.0171	1.0174
0.5	0.0370	0.1467	0.2161	0.2991	0.1946	0.1079	0.0098	0.0130	1.0241
0.6	0.0395	0.1641	0.2400	0.3365	0.1726	0.0860	-0.0321	0.0266	1.0332
0.7	0.0421	0.1839	0.2666	0.3799	0.1296	0.0657	-0.0878	0.0779	1.0579
0.8	0.0448	0.2059	0.2954	0.4290	0.0575	0.0580	-0.1661	0.1998	1.1244
0.9	0.0477	0.2299	0.3259	0.4839	-0.0531	0.0804	-0.2856	0.4476	1.2767
1.0	0.0506	0.2557	0.3578	0.5446	-0.2129	0.1586	-0.4812	0.9139	1.5870

← Largest α without negative values (α=0.5)

Difference between the Sum(φ) and 1 is the error.

Error = 2.4%

Supplementary Figure 5 | An example of calculating η from λ and φ. a, This example is similar to that in Supplementary Figure 4. Here, each time we discover another value of η we must remember to subtract the multi-weighted convolutions (as in Supplementary Figure 3) of the incomplete η from λ. **b,** Shown is the explicit example of searching a normalized exponential distribution of η by varying the rate parameter α. When the deconvolution was performed with rate parameter α=0.5, the first negative number appeared at φ(6). All larger rate parameters contain negative values. The error for this distribution was calculated as the difference in its sum from 1.

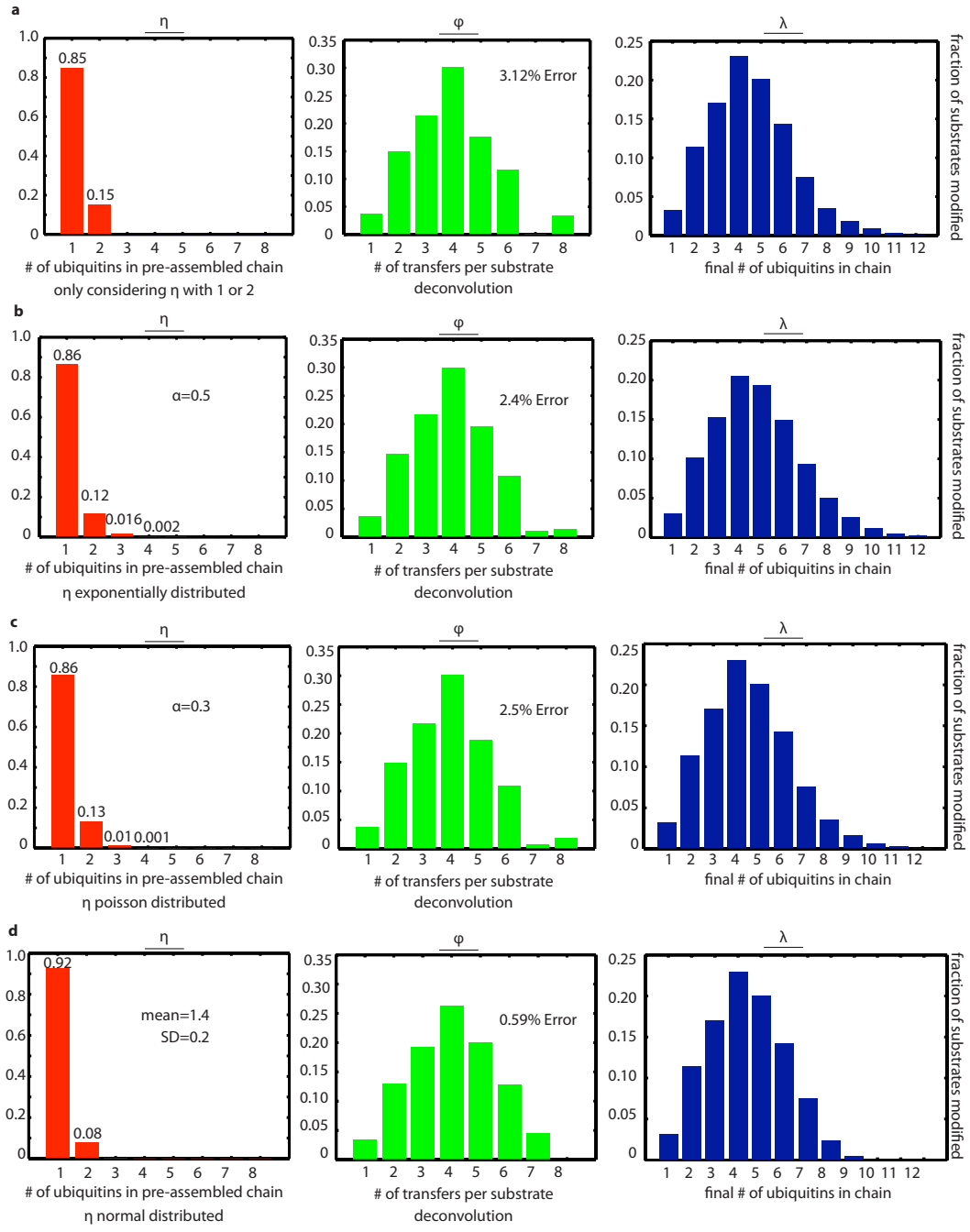

Supplementary Figure 6 | Deconvolution of φ from λ_{CycE}. a, Considering distributions of η that only contain η(1) and η(2), φ was calculated by deconvolution with λ_{CycE}. The distribution shown was that which deviated most from η(1)=100% whose φ did not contain values >1 or <0 and that when convoluted with φ, the sum fell within 0.95 and 1.05, or an error rate of ± 5%. **b,** Considering distributions of η that were exponentially distributed with rate parameter α. **c,** Considering distributions of η that were poisson distributed with average α. **d,** Considering distributions of η that were normal distributed varying the mean and SD. Random distributions were also considered (data not shown).

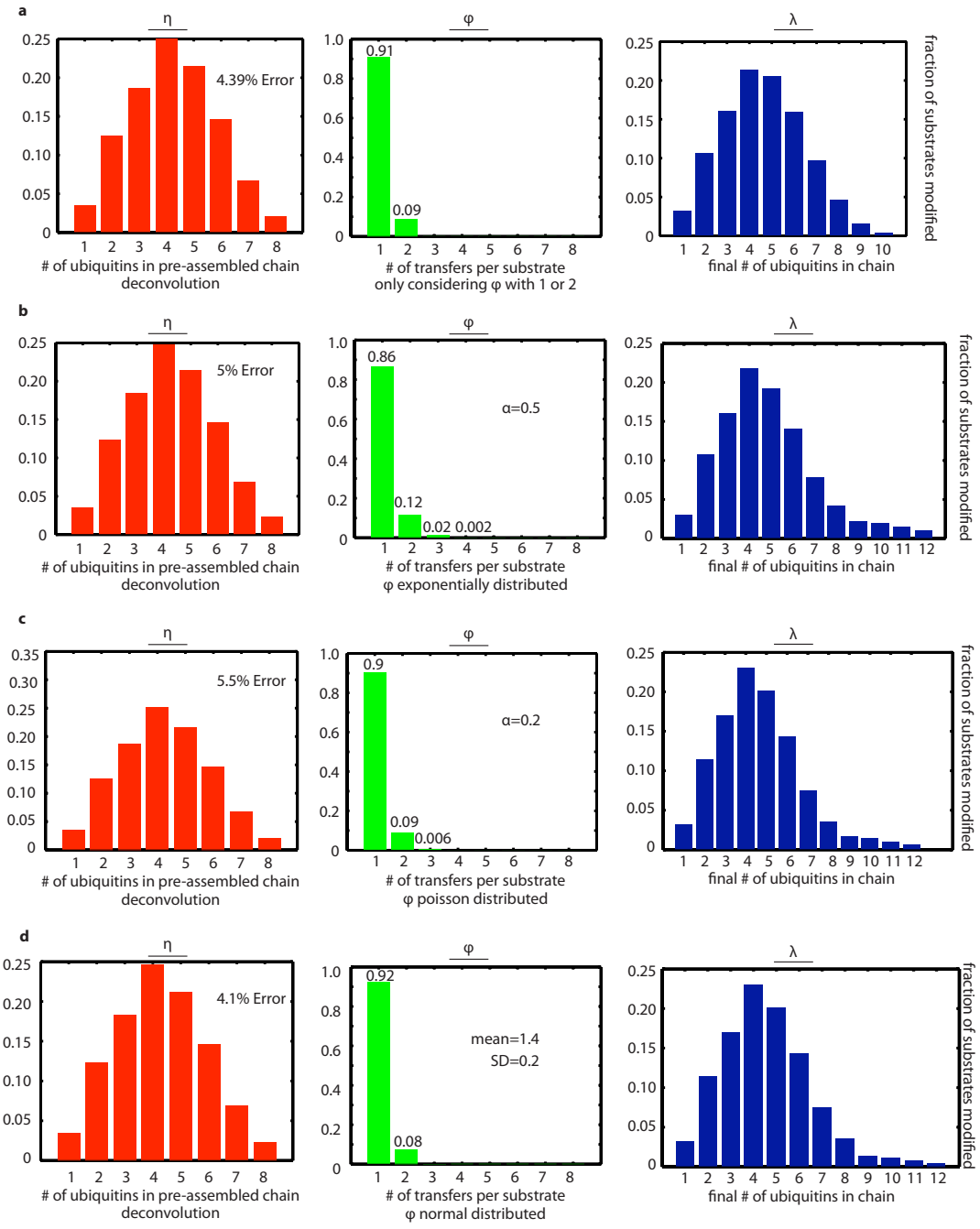

Supplementary Figure 7 | Deconvolution of η from λ_{CycE}. a, Considering distributions of φ that only contain φ(1) and φ (2), η was calculated by deconvolution with λ_{CycE}. The distribution shown was that which deviated most from φ(1)=100% whose η did not contain values >1 or <0 and that when convoluted with η, the sum fell within 0.95 and 1.05, or an error rate of ± 5%. **b,** Considering distributions of φ that were exponentially distributed with rate parameter α. **c,** Considering distributions of φ that were poisson distributed with average α. **d,** Considering distributions of φ that were normal distributed varying the mean and SD. Random distributions were also considered (data not shown).

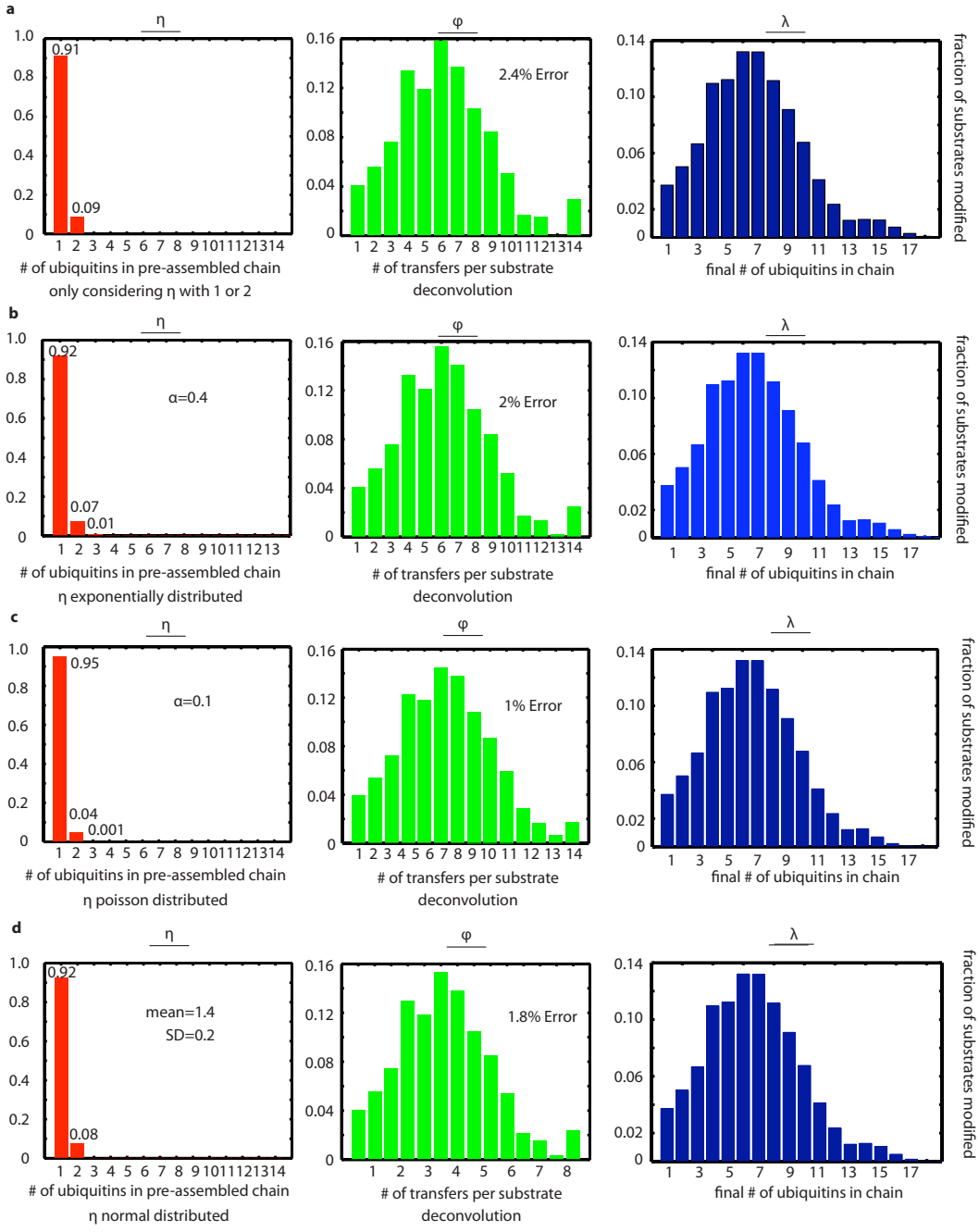

Supplementary Figure 8 | Deconvolution of φ from $\lambda_{\beta\text{-Cat}}$. a, Considering distributions of η that only contain η(1) and η(2), φ was calculated by deconvolution with $\lambda_{\beta\text{-Cat}}$. The distribution shown was that which deviated most from η(1)=100% whose φ did not contain values >1 or <0 and that when convoluted with φ, the sum fell within 0.95 and 1.05, or an error rate of ± 5%. **b,** Considering distributions of η that were exponentially distributed with rate parameter α. **c,** Considering distributions of η that were poisson distributed with average α. **d,** Considering distributions of η that were normal distributed varying the mean and SD. Random distributions were also considered (data not shown).

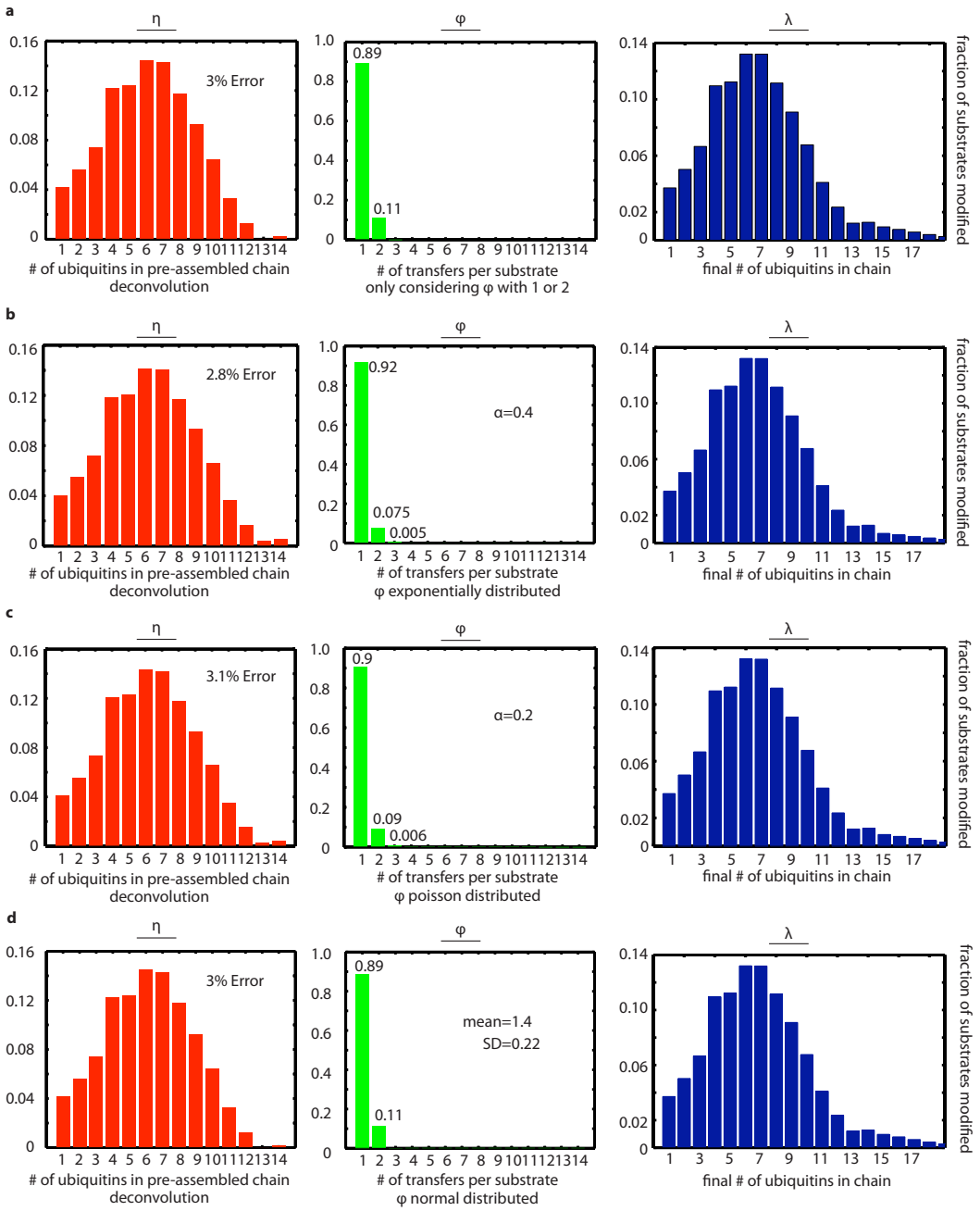

Supplementary Figure 9 | Deconvolution of η from $\lambda_{\beta\text{-Cat}}$. a, Considering distributions of φ that only contain φ(1) and φ (2), η was calculated by deconvolution with $\lambda_{\beta\text{-Cat}}$. The distribution shown was that which deviated most from φ(1)=100% whose η did not contain values >1 or <0 and that when convoluted with η, the sum fell within 0.95 and 1.05, or an error rate of ± 5%. **b,** Considering distributions of φ that were exponentially distributed with rate parameter α. **c,** Considering distributions of φ that were poisson distributed with average α. **d,** Considering distributions of φ that were normal distributed varying the mean and SD. Random distributions were also considered (data not shown).

a

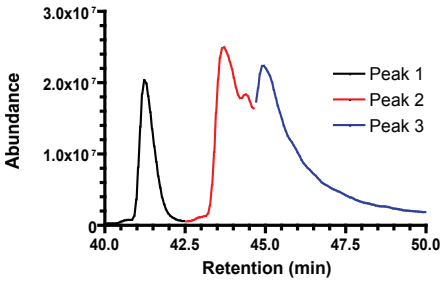

b

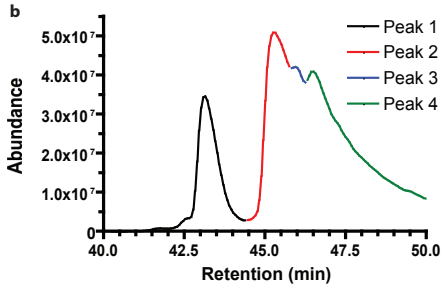

c

Protein	Mass (theoretical)	Mass (measured)	Abudance	Peak
Ubiquitin	8565	8565	1,250,158	1
Cdc34~Ub	40,792	40,792	838,665	2
		41,830	137,725	2
		40,787	204,375	3
		60,559	170,061	3
		104,033	147,021	3
		106,823	144,456	3
		88,303	142,422	3
		107,237	134,176	3
		80,790	134,085	3
		106,427	130,900	3
		89,100	125,780	3
		79,957	124,787	3

d

Protein	Mass (theoretical)	Mass (measured)	Abudance	Peak
Ubiquitin	8565	8564	1,448,614	1
Ub-DTT	8701	8701	627,263	1
Cdc34~Ub	40,792	40,789	2,267,926	2
Cdc34~Ub	40,792	40,790	1,217,040	3
Cdc34	32,245	32,242	145,616	3
Cdc34~Ub	40,792	40,788	471,765	4
Cdc34	32,245	32,243	326,504	4
		60,570	176,801	4
		80,775	156,325	4
		79,940	153,394	4
		60,129	144,097	4
		61,003	116,335	4
		61,460	112,311	4
		59,775	103,833	4
		79,121	97,101	4

Supplementary Figure 10 | Mass spectrometry analysis of Cdc34. a, Chromatograms of mass spectrometry analysis of reaction containing Uba1, yeast Cdc34 and ubiquitin in the presence of ATP. Where possible, species are identified and the masses are compared with the theoretical value. Peak 3 contains multiple species including Uba1 and impurities. The theoretical masses for Cdc34~Ub2 (49,338), Cdc34~Ub3 (57,886), Cdc34~Ub4 (66,433) are not observed. **b,** Chromatograms of mass spectrometry analysis of reaction containing Uba1, yeast Cdc34 and ubiquitin (Ub) in the presence of ATP and SCF^{Cdc4}. Where possible, species are identified and the masses are compared with the theoretical value. Peak 4 contains multiple species including E1 and impurities. **c,** Analysis of peaks from a. **d,** Analysis of peaks from b.

a

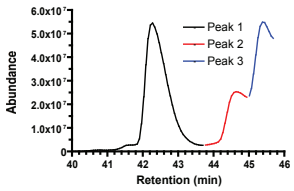

b

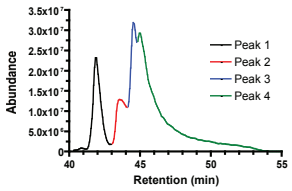

c

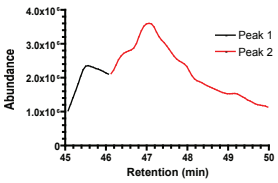

d

Protein	Mass (theoretical)	Mass (measured)	Abudance	Peak
Ub-DTT	8701	8701	4,004,748	1
Cdc34~Ub	40,792	40,790	856,005	2
Cdc34	32,245	32,243	2,104,438	3

e

Protein	Mass (theoretical)	Mass (measured)	Abudance	Peak
Di-ubiquitin	17,111	17,093	1,219,060	1
Cdc34~Ub2	49,338	49,339	358,429	2
Cdc34	32,245	32,244	1,056,240	3
Cdc34	32,245	32,243	342,426	4
		114,412	141,956	4
		113,442	131,956	4
		55,481	113,943	4
		115,141	112,219	4
		55,890	111,557	4
		56,788	106,226	4
		112,563	87,983	4
		37,546	87,790	4
		44,326	81,153	4

f

Protein	Mass (theoretical)	Mass (measured)	Abudance	Peak
		16,951	20,405	1
		40,816	13,500	1
		16,991	10,620	1
		16,977	9,508	1
		40,861	8524	1
		17,008	6,772	1
		41,838	6,612	1
		40,900	6,249	1
		36,023	6,204	1
		78,867	6,008	1
		109,318	20,828	2
		109,554	20,484	2
		98,618	19,802	2
		66,153	18,346	2
		61,032	18,301	2
		88,227	17,086	2
		37,291	15,688	2
		52,670	15,672	2
		64,288	15,270	2
		80,111	15,003	2

Supplementary Figure 11 | Mass spectrometry analysis of Cdc34 controls. a, Chromatograms of mass spectrometry analysis of reaction containing E1, Cdc34 and ubiquitin (Ub) in the presence of ATP, SCF and DTT. Where possible, species are identified and the masses are compared with the theoretical value. **b,** Chromatograms of mass spectrometry analysis of reaction containing E1, Cdc34 and K48 di-ubiquitin in the presence of ATP. Where possible, species are identified and the masses are compared with the theoretical value. Peak 4 contains multiple species including E1 and impurities. **c,** Chromatograms of mass spectrometry analysis of SCF^{Cdc4} in reaction buffer. **d,** Analysis of peaks from a. **e,** Analysis of peaks from b. **f,** Analysis of peaks from c.

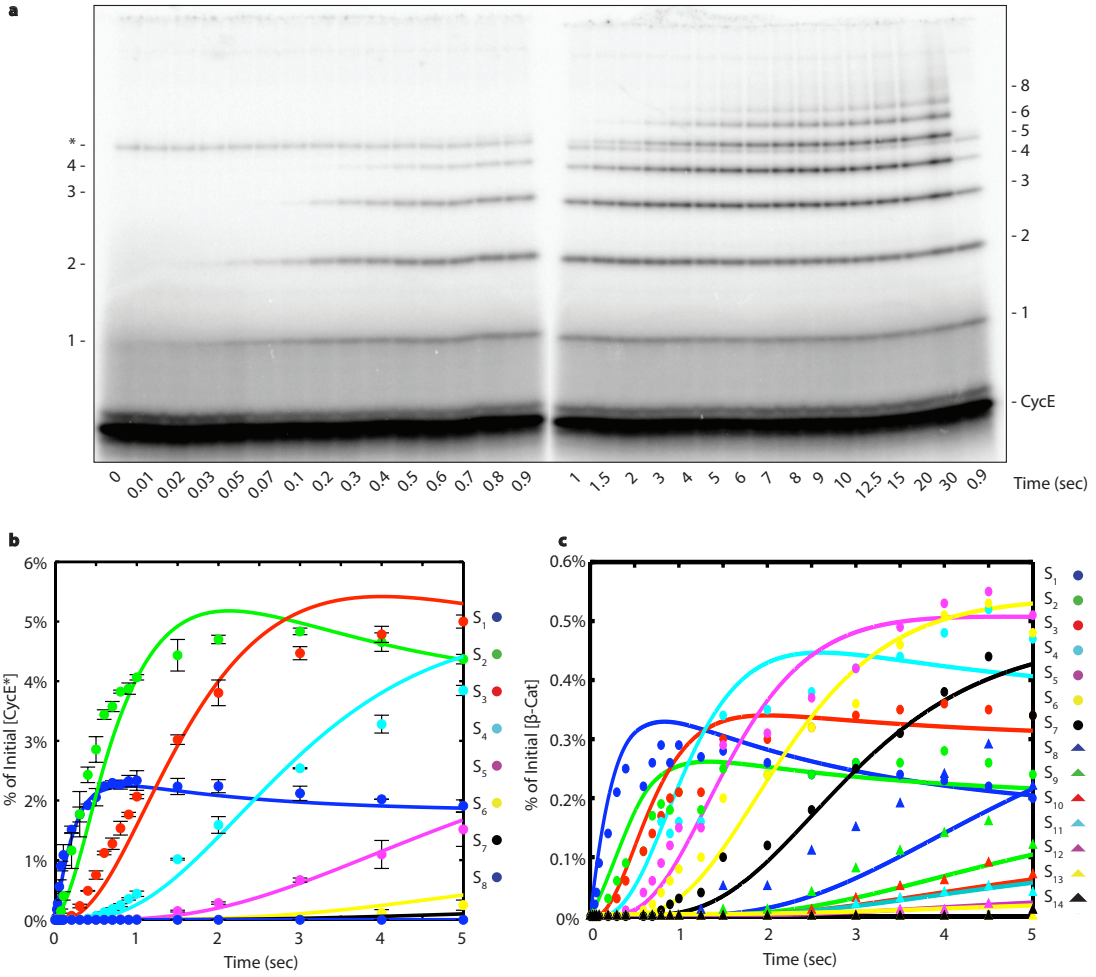

Supplementary Figure 12 | Millisecond kinetics of a single encounter reaction. a, Samples from the same reaction shown in Fig. 2a were run on a 12-24% tricine gel to optimize detection and quantification of S2 and S5. The asterisk marks an unreactive contaminant of the labeled CycE. **b,** A zoomed plot of Fig. 3b up to 5 seconds. The error of each fit is shown in Supplementary Figure 14. **c,** A zoomed plot of Fig. 3e up to 5 seconds. The error of each fit is shown in Supplementary Figure 15.

Analytical Closed Form Solutions

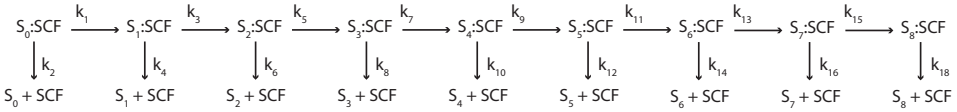

[SCF:S0] = 61.5% at t=0

$$[S_0] = 61.5\left(1-\frac{k_2}{k_1+k_2}\right)e^{-(k_1+k_2)t} + 61.5\frac{k_2}{k_1+k_2} + (100-61.5)$$

$$[S_1]_{Total} = 61.5\,k_1\left(\frac{e^{-(k_1+k_2)t}}{(k_3+k_4)-(k_1+k_2)} + \frac{e^{-(k_3+k_4)t}}{(k_1+k_2)-(k_3+k_4)}\right) + 61.5\left(\frac{k_1}{k_1+k_2}\right)\left(\frac{k_4}{k_3+k_4}\right)\left(1-\frac{(k_3+k_4)e^{-(k_1+k_2)t}}{(k_3+k_4)-(k_1+k_2)} - \frac{(k_1+k_2)e^{-(k_3+k_4)t}}{(k_1+k_2)-(k_3+k_4)}\right)$$

$$[S_2]_{Total} = 61.5\,k_1k_3\left(\frac{e^{-(k_1+k_2)t}}{((k_3+k_4)-(k_1+k_2))((k_5+k_6)-(k_1+k_2))} + \frac{e^{-(k_3+k_4)t}}{((k_1+k_2)-(k_3+k_4))((k_5+k_6)-(k_3+k_4))} + \frac{e^{-(k_5+k_6)t}}{((k_1+k_2)-(k_5+k_6))((k_3+k_4)-(k_5+k_6))}\right)$$

$$+ 61.5\left(\frac{k_1}{k_1+k_2}\right)\left(\frac{k_3}{k_3+k_4}\right)\left(\frac{k_6}{k_5+k_6}\right)\left(1-\frac{(k_3+k_4)(k_5+k_6)e^{-(k_1+k_2)t}}{((k_3+k_4)-(k_1+k_2))((k_5+k_6)-(k_1+k_2))} - \frac{(k_1+k_2)(k_5+k_6)e^{-(k_3+k_4)t}}{((k_1+k_2)-(k_3+k_4))((k_5+k_6)-(k_3+k_4))} - \frac{(k_1+k_2)(k_3+k_4)e^{-(k_5+k_6)t}}{((k_1+k_2)-(k_5+k_6))((k_3+k_4)-(k_5+k_6))}\right)$$

$$[S_{n/2}]_{Total} = 61.5\,k_1k_3\ldots k_{n-1}\left(\frac{e^{-(k_1+k_2)t}}{((k_3+k_4)-(k_1+k_2))((k_5+k_6)-(k_1+k_2))\ldots((k_{n-1}+k_n)-(k_1+k_2))} + \frac{e^{-(k_3+k_4)t}}{((k_1+k_2)-(k_3+k_4))((k_5+k_6)-(k_3+k_4))\ldots((k_{n-1}+k_n)-(k_3+k_4))}\right.$$

$$\left. + \ldots + \frac{e^{-(k_{n-1}+k_n)t}}{((k_1+k_2)-(k_{n-1}+k_n))((k_3+k_4)-(k_{n-1}+k_n))\ldots((k_{n-3}+k_{n-2})-(k_{n-1}+k_n))}\right)$$

$$+ 61.5\left(\frac{k_1}{k_1+k_2}\right)\left(\frac{k_3}{k_3+k_4}\right)\cdots\left(\frac{k_n}{k_{n-1}+k_n}\right)\left(1-\frac{(k_3+k_4)(k_5+k_6)\ldots(k_{n-1}+k_n)e^{-(k_1+k_2)t}}{((k_3+k_4)-(k_1+k_2))((k_5+k_6)-(k_1+k_2))\ldots((k_{n-1}+k_n)-(k_1+k_2))} - \frac{(k_1+k_2)(k_5+k_6)\ldots(k_{n-1}+k_n)e^{-(k_3+k_4)t}}{((k_1+k_2)-(k_3+k_4))((k_5+k_6)-(k_3+k_4))\ldots((k_{n-1}+k_n)-(k_3+k_4))}\right.$$

$$\left. - \frac{(k_1+k_2)(k_3+k_4)\ldots(k_{n-3}+k_{n-2})e^{-(k_{n-1}+k_n)t}}{((k_1+k_2)-(k_{n-1}+k_n))((k_3+k_4)-(k_{n-1}+k_n))\ldots((k_{n-3}+k_{n-2})-(k_{n-1}+k_n))}\right)$$

Supplementary Figure 13 | Closed form solutions to a kinetic model of a single encounter reaction with η(1)=100%. The analytical solutions were calculated using the method of Laplace transforms. Each new species contributed two new rate constants to the overall scheme.

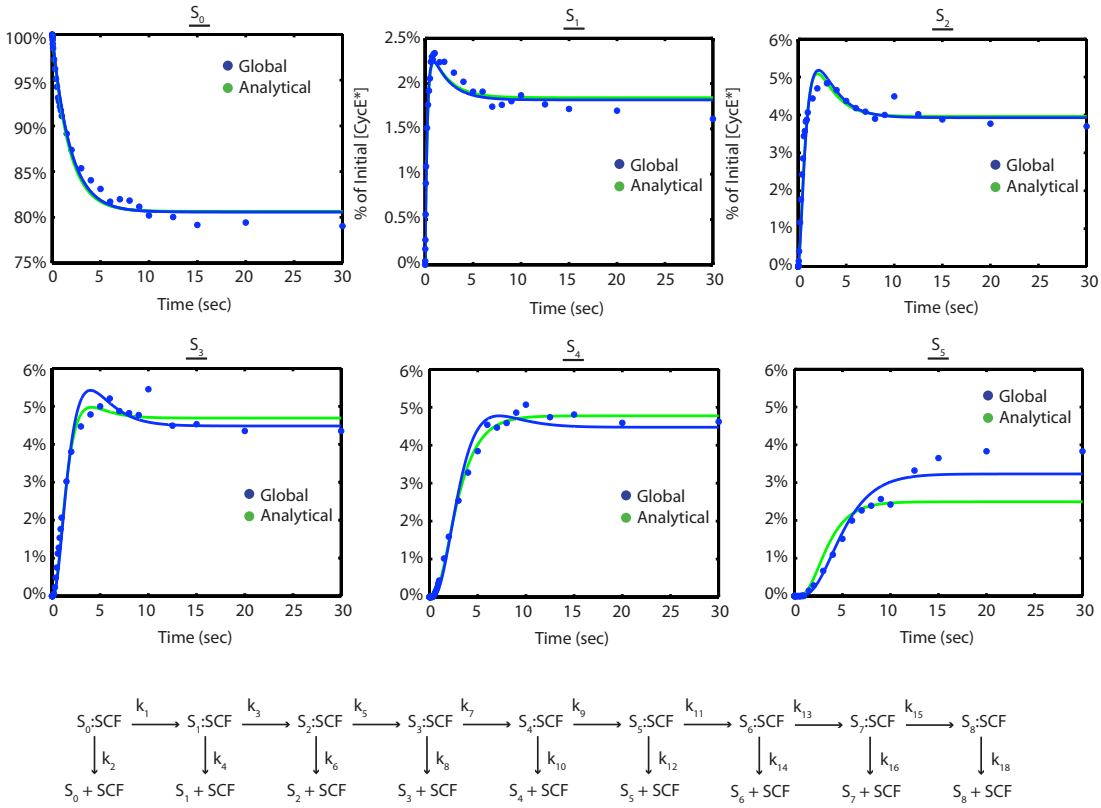

Global Analysis Solutions

$k_1 = 0.17\ s^{-1}$	Standard Error = 0.00913
$k_2 = 0.37\ s^{-1}$	Standard Error = 0.0254
$k_3 = 3.8\ s^{-1}$	Standard Error = 0.3056
$k_4 = 0.40\ s^{-1}$	Standard Error = 0.0472
$k_5 = 1.0\ s^{-1}$	Standard Error = 0.124
$k_6 = 0.29\ s^{-1}$	Standard Error = 0.0497
$k_7 = 0.55\ s^{-1}$	Standard Error = 0.0942
$k_8 = 0.27\ s^{-1}$	Standard Error = 0.0617
$k_9 = 0.31\ s^{-1}$	Standard Error = 0.0968
$k_{10} = 0.29\ s^{-1}$	Standard Error = 0.118
$k_{11} = 0.41\ s^{-1}$	Standard Error = 0.783
$k_{12} = 0.89\ s^{-1}$	Standard Error = 1.782

Analytical Closed Form Solutions

$k_1 = 0.1829\ s^{-1}$	95% CI = (0.165, 0.2009)	R-square = 0.9876
$k_2 = 0.3986\ s^{-1}$	95% CI = (0.3504, 0.4467)	RMSE = 0.8744
$k_3 = 3.84\ s^{-1}$	95% CI = (3.638, 4.043)	R-square = 0.9787
$k_4 = 0.3931\ s^{-1}$	95% CI = (0.364, 0.4222)	RMSE = 0.1051
$k_5 = 1.111\ s^{-1}$	95% CI = (0.9352, 1.287)	R-square = 0.9607
$k_6 = 0.3238\ s^{-1}$	95% CI = (0.364, 0.3882)	RMSE = 0.3556
$k_7 = 0.8001\ s^{-1}$	95% CI = (0.6324, 0.9678)	R-square = 0.984
$k_8 = 0.4218\ s^{-1}$	95% CI = (0.3188, 0.5249)	RMSE = 0.2736
$k_9 = 1.619\ s^{-1}$	95% CI = (0.8376, 2.913)	R-square = 0.9969
$k_{10} = 1.876\ s^{-1}$	95% CI = (0.7496, 2.489)	RMSE = 0.1204
$k_{11} = 59.67\ s^{-1}$	95% CI = (-3841, 3960)	R-square = 0.9896
$k_{12} = 91.47\ s^{-1}$	95% CI = (-5891, 6074)	RMSE = 0.1427

Supplementary Figure 14 | Comparison of rate constants estimated from analytical solutions and global regression for CycE. Comparison of the analytical and globally refined rate constants revealed that the global analysis helped to correct for the error accumulation in the analytical regression.

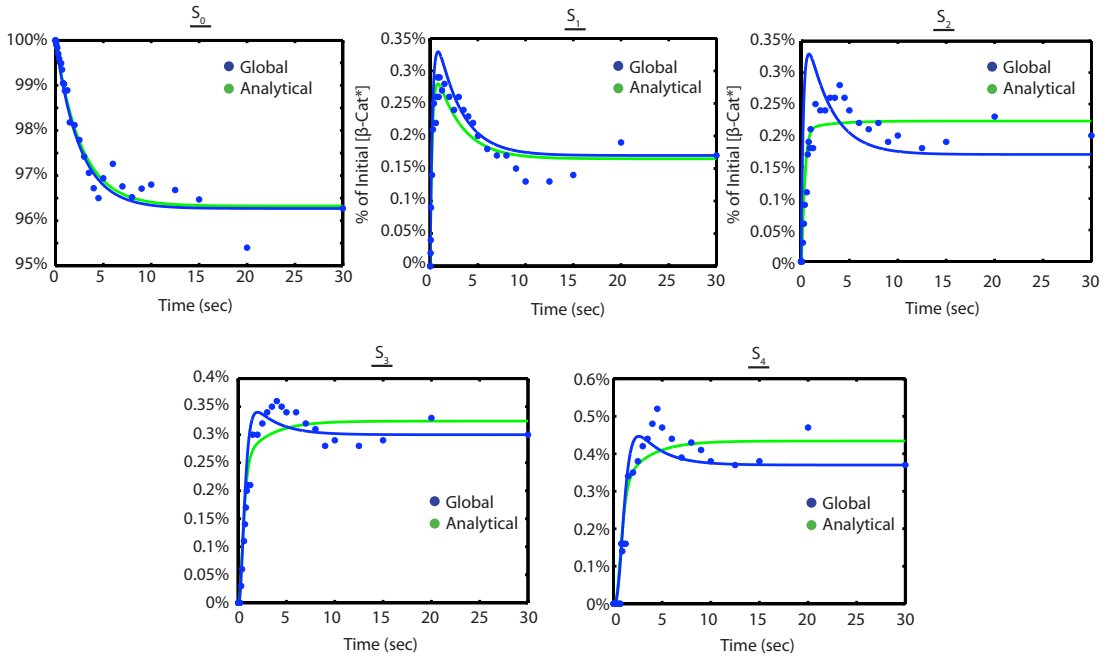

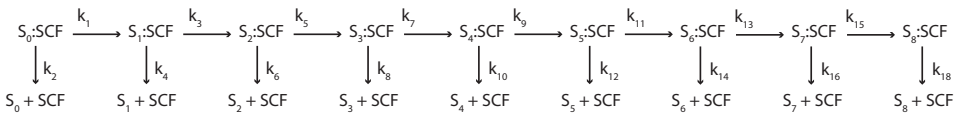

Global Analysis Solutions

k_1 = 0.03 s^{-1}	Standard Error = 0.00261
k_2 = 0.363 s^{-1}	Standard Error = 0.0313
k_3 = 3.58 s^{-1}	Standard Error = 0.627
k_4 = 0.171 s^{-1}	Standard Error = 0.0299
k_5 = 4.45 s^{-1}	Standard Error = 1.1
k_6 = 0.265 s^{-1}	Standard Error = 0.0658
k_7 = 3.22 s^{-1}	Standard Error = 0.802
k_8 = 0.315 s^{-1}	Standard Error = 0.0786
k_9 = 2 s^{-1}	Standard Error = 0.481
k_{10} = 0.275 s^{-1}	Standard Error = 0.0661
k_{11} = 1.63 s^{-1}	Standard Error = 0.420
k_{12} = 0.372 s^{-1}	Standard Error = 0.0959
k_{13} = 1.21 s^{-1}	Standard Error = 0.382
k_{14} = 0.395 s^{-1}	Standard Error = 0.125
k_{15} = 1.01 s^{-1}	Standard Error = 0.571
k_{16} = 0.467 s^{-1}	Standard Error = 0.241

Analytical Closed Form Solutions

k_1 = 0.02839 s^{-1}	95% CI = (0.02413, 0.03266)	R-square = 0.9634
k_2 = 0.3463 s^{-1}	95% CI = (0.2797, 0.413)	RMSE = 0.2822
k_3 = 4.098 s^{-1}	95% CI = (3.757, 4.44)	R-square = 0.9112
k_4 = 0.1926 s^{-1}	95% CI = (0.1628, 0.2224)	RMSE = 0.0256
k_5 = 5.849 s^{-1}	95% CI = (4.942, 6.755)	R-square = 0.8988
k_6 = 0.1926 s^{-1}	95% CI = (0.3149, 0.479)	RMSE = 0.03
k_7 = 4.278 s^{-1}	95% CI = (3.614, 4.943)	R-square = 0.9488
k_8 = 0.4682 s^{-1}	95% CI = (0.3779, 0.5585)	RMSE = 0.03099
k_9 = 2.927 s^{-1}	95% CI = (2.092, 3.763)	R-square = 0.9209
k_{10} = 0.5024 s^{-1}	95% CI = (0.3304, 0.6743)	RMSE = 0.05625

Supplementary Figure 15 | Comparison of rate constants estimated from analytical solutions and global regression for β-Cat. Comparison of the analytical and globally refined rate constants revealed that the global analysis helped to correct for the error accumulation in the analytical regression. The error for the β-Cat regressions are higher versus the CycE regression because of reduced fraction of substrate converted.

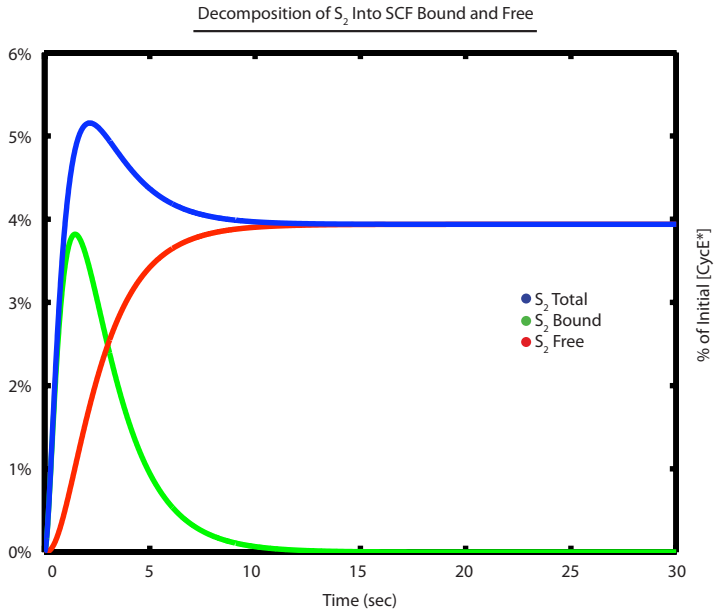

$$[S_2]_{Total} = [S_2]bound + [S_2]free = 61.5\,k_1k_3\left(\frac{e^{-(k_1+k_2)t}}{((k_3+k_4)-(k_1+k_2))((k_5+k_6)-(k_1+k_2))}+\frac{e^{-(k_3+k_4)t}}{((k_1+k_2)-(k_3+k_4))((k_5+k_6)-(k_3+k_4))}+\frac{e^{-(k_5+k_6)t}}{((k_1+k_2)-(k_5+k_6))((k_3+k_4)-(k_5+k_6))}\right)$$

$$+61.5\left(\frac{k_1}{k_1+k_2}\right)\left(\frac{k_3}{k_3+k_4}\right)\left(\frac{k_6}{k_5+k_6}\right)\left(1-\frac{(k_3+k_4)(k_5+k_6)e^{-(k_1+k_2)t}}{((k_3+k_4)-(k_1+k_2))((k_5+k_6)-(k_1+k_2))}-\frac{(k_1+k_2)(k_5+k_6)e^{-(k_3+k_4)t}}{((k_1+k_2)-(k_3+k_4))((k_5+k_6)-(k_3+k_4))}-\frac{(k_1+k_2)(k_3+k_4)e^{-(k_5+k_6)t}}{((k_1+k_2)-(k_5+k_6))((k_3+k_4)-(k_5+k_6))}\right)$$

Supplementary Figure 16 | Overshoot behavior reveals flux through each species. Using the analytical solutions, the overshoot behavior was directly correlated to the amount of flux through each species. Each curve may be dissected into the substrate that was bound to SCF or free at the time of quench. The sum of these two species gives the measured curve.

Appendix B: Supplementary Materials for Chapter 3

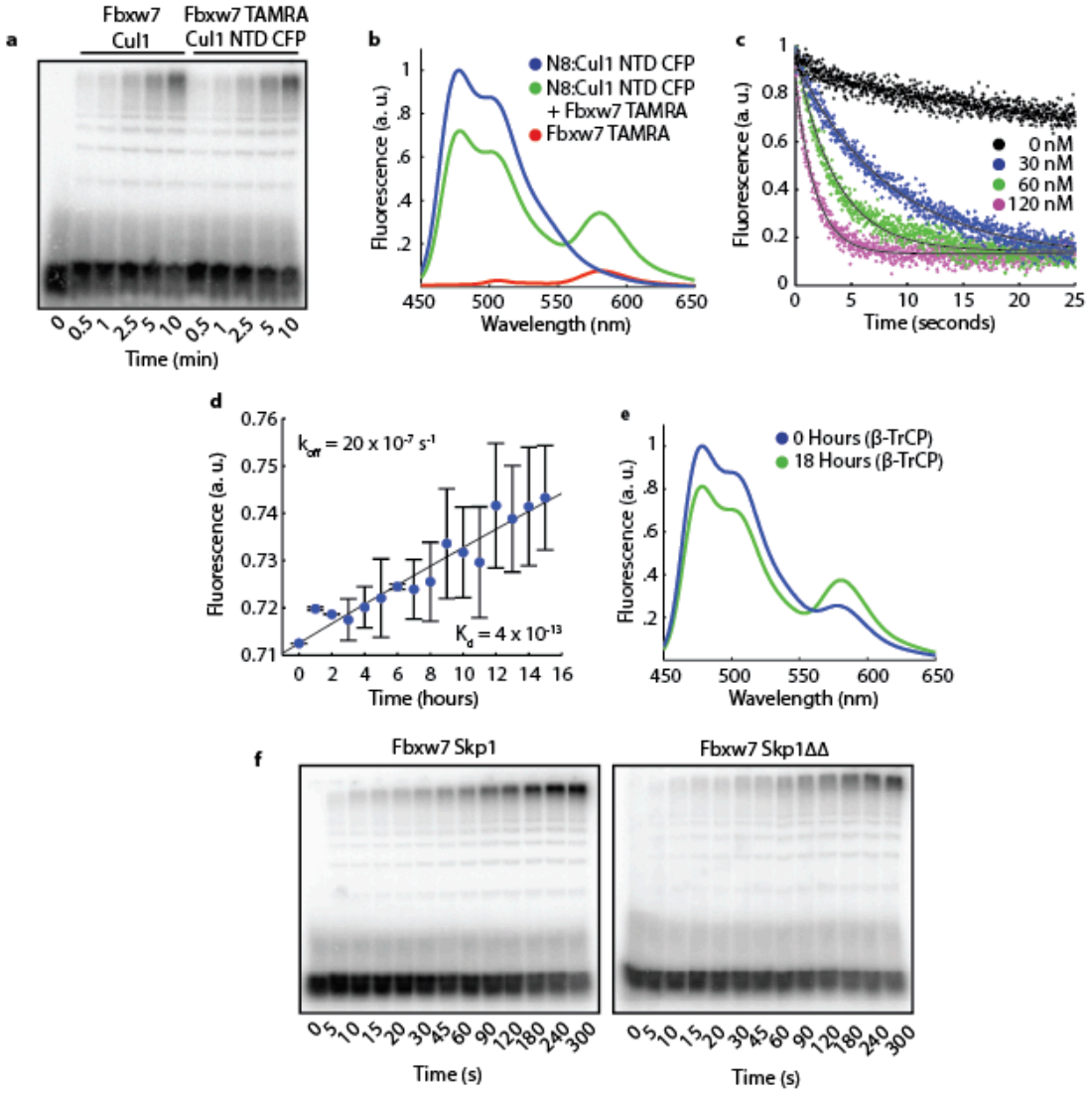

Supplementary Figure 1 | a, 600 nM radiolabeled CycE was pre-incubated with either 150 nM Cul1/Rbx1/Fbxw7/Skp1 or 150 nM Cul1 NTD CFP/Rbx1/Fbxw7 TAMRA/Skp1 and then mixed with 10 μM Cdc34b, 1 μM Ub E1, and 60 μM Ub. **b,** As in Fig. 1a except with 70 nM neddylated Cul1 NTD CFP. **c,** As in Fig. 1b except with 5 nM neddylated Cul1 NTD CFP. **d,** As in Fig. 1e except with 70 nM neddylated Cul1 NTD CFP. **e,** Scans from indicated time points in Fig. 1f. **f,** As in Supplementary Fig. 1a except with Fbxw7/Skp1 or Fbxw7/Skp1ΔΔ.

Bibliography

Bai C, Sen P, Hofmann K, Ma L, Goebl M, Harper JW, Elledge SJ (2006). SKP1 connects cell cycle regulators to the ubiquitin proteolysis machinery through a novel motif, the F-box. *Cell*. 86(2):263-74.

Bennett EJ, Rush J, Gygi SP, Harper JW (2010). Dynamics of cullin-RING ubiquitin ligase network revealed by systematic quantitative proteomics. *Cell.* 143(6):951-65.

Chau V, Tobias JW, Bachmair A, Marriott D, Ecker DJ, Gonda DK, Varshavsky A (1989). A multiubiquitin chain is confined to specific lysine in a targeted short-lived protein. *Science.* 243(4898):1576-83.

Chuang HW, Zhang W, Gray WM (2004). Arabidopsis ETA2, an apparent ortholog of the human cullin-interacting protein CAND1, is required for auxin responses mediated by the SCF(TIR1) ubiquitin ligase. *Plant Cell.* 16(7):1883-97.

Ciehanover A, Hod Y, Hershko A. (1978) A heat-stable polypeptide component of an ATP-dependent proteolytic system from reticulocytes. *Biochem Biophys Res Commun*. 81(4):1100-5.

Cope GA, Deshaies RJ (2002). COP9 signalosome: a multifunctional regulator of SCF and other cullin-based ubiquitin ligases. *Cell.* 114(6):663-71.

Deng L, Wang C, Spencer E, Yang L, Braun A, You J, Slaughter C, Pickart C, Chen ZJ (2000). Activation of the IkappaB kinase complex by TRAF6 requires a dimeric ubiquitin-conjugating enzyme complex and a unique polyubiquitin chain. *Cell*. 103(2):351-61.

Deshaies RJ, Joazeiro CA (2009). RING domain E3 ubiquitin ligases. *Annu Rev Biochem.* 78: 399-434.

Duda DM, Borg LA, Scott DC, Hunt HW, Hammel M, Schulman BA (2008). Structural insights into NEDD8 activation of cullin-RING ligases: conformational control of conjugation. *Cell.* 134(6):995-1006.

Dye BT, Schulman BA (2007). Structural mechanisms underlying posttranslational modification by ubiquitin-like proteins. *Annual Review of Biophysics and Biomolecular Structure.* 36: 131-50.

Feldman RM, Correll CC, Kaplan KB, Deshaies RJ (1997). A complex of Cdc4p, Skp1p, and Cdc53p/cullin catalyzes ubiquitination of the phosphorylated CDK inhibitor Sic1p. *Cell*. 91: 221-30.

Feng S, Shen Y, Sullivan JA, Rubio V, Xiong Y, Sun TP, Deng XW (2004). Arabidopsis CAND1, an unmodified CUL1-interacting protein, is involved in multiple developmental pathways controlled by ubiquitin/proteasome-mediated protein Degradation. *Plant Cell.* 16(7):1870-82.

Fersht, A. (1999). *Structure And Mechanism In Protein Science: A Guide To Enzyme Catalysis And Protein Folding.* New York: W. H. Freeman and Company.

Goldenberg SJ, Cascio TC, Shumway SD, Garbutt KC, Liu J, Xiong Y, Zheng N (2004). Structure of the Cand1-Cul1-Roc1 complex reveals regulatory mechanisms for the assembly of the multisubunit cullin-dependent ubiquitin ligases. *Cell*. 119(4):517-28.

Goldknopf IL, Busch H. (1977). Isopeptide linkage between nonhistone and histone 2A polypeptides of chromosomal conjugate-protein A24. *Proc Natl Acad Sci U S A*. 74(3):864-8.

Goldstein G, Scheid M, Hammerling U, Schlesinger DH, Niall HD, Boyse EA. (1975). Isolation of a polypeptide that has lymphocyte-differentiating properties and is probably represented universally in living cells. *Proc Natl Acad Sci U S A.* 72(1):11-5

Haas AL, Warms JV, Hershko A, Rose IA. (1982). Ubiquitin-activating enzyme. Mechanism and role in protein-ubiquitin conjugation. *J Biol Chem.* 10;257(5):2543-8.

Hershko A, Ciechanover A, Heller H, Haas AL, Rose IA. (1980). Proposed role of ATP in protein breakdown: conjugation of protein with multiple chains of the polypeptide of ATP-dependent proteolysis. *Proc Natl Acad Sci U S A.* 1980 Apr;77(4):1783-6.

Hershko A, Ciechanover A, Rose IA. (1981). Identification of the active amino acid residue of the polypeptide of ATP-dependent protein breakdown. *J Biol Chem*. 256(4):1525-8.

Hochstrasser, M. (2006). Lingering Mysteries of Ubiquitin-Chain Assembly. *Cell*. 124: 27-34.

Jin J, Li X, Gygi SP, Harper JW. (2007) Dual E1 activation systems for ubiquitin differentially regulate E2 enzyme charging. *Nature.* 447(7148):1135-8.

Jin L, Williamson A, Banerjee S, Philipp I, Rape M (2008). Mechanism of ubiquitin-chain formation by the human anaphase-promoting complex. *Cell.* 133(4):653-65.

Kamura T, Conrad MN, Yan Q, Conaway RC, Conaway JW. (1999). The Rbx1 subunit of SCF and VHL E3 ubiquitin ligase activates Rub1 modification of cullins Cdc53 and Cul2. *Genes & Development*. 13: 2928-2933.

Kati WM, Johnson KA, Jerva LF, Anderson KS. (1992). Mechanism and fidelity of HIV reverse transcriptase. *J Biol Chem*. 267: 25988-97.

Kleiger G, Saha A, Lewis S, Kuhlman B, Deshaies RJ (2009). Rapid E2-E3 assembly and disassembly enable processive ubiquitylation of cullin-RING ubiquitin ligase substrates. *Cell.* 139(5):957-68.

Lee JE, Sweredoski MJ, Graham RL, Kolawa NJ, Smith GT, Hess S, Deshaies RJ (2011). The steady-state repertoire of human SCF ubiquitin ligase complexes does not require ongoing Nedd8 conjugation. *Mol Cell Proteomics.* 10(5):M110.006460.

Li W, Tu D, Brunger AT, Ye Y. (2007). A ubiquitin ligase transfers preformed polyubiquitin chains from a conjugating enzyme to a substrate. *Nature*. 446: 333-337.

Li W, Tu D, Li L, Wollert T, Ghirlando R, Brunger AT, Ye Y. (2009). Mechanistic insights into active site-associated polyubiquitination by the ubiquitin-conjugating enzyme Ube2g2. *Proc Natl Acad Sci USA*. 106: 3722-7.

Liu J, Furukawa M, Matsumoto T, Xiong Y (2002). NEDD8 modification of CUL1 dissociates p120(CAND1), an inhibitor of CUL1-SKP1 binding and SCF ligases. *Mol Cell.* 10(6):1511-8.

Lo SC, Hannink M (2006). CAND1-mediated substrate adaptor recycling is required for efficient repression of Nrf2 by Keap1. *Mol Cell Biol*. 26(4):1235-44.

Nash P, Tang X, Orlicky S, Chen Q, Gertler FB, Mendenhall MD, Sicheri F, Pawson T, Tyers M. (2001). Multisite phosphorylation of a CDK inhibitor sets a threshold for the onset of DNA replication. *Nature.* 414: 514-21.

Orlicky S, Tang X, Willems A, Tyers M, Sicheri F. (2003). Structural basis for phosphodependent substrate selection and orientation by the SCFCdc4 ubiquitin ligase. *Cell.* 112: 243-56.

Petroski MD, Deshaies RJ (2005a). Function and regulation of cullin–RING ubiquitin ligases. *Nat Rev Mol Cell Biol.* 6: 9-20.

Petroski MD, Deshaies RJ (2005b). Mechanism of Lysine 48-Linked Ubiquitin-Chain Synthesis by the Cullin-RING Ubiquitin-Ligase Complex SCF-Cdc34. *Cell.* 123: 1107-1120.

Petroski MD, Deshaies RJ (2005c). In Vitro Reconstitution of SCF Substrate Ubiquitination with Purified Proteins. *Methods in Enzymology*. 398: 143-158.

Petroski MD, Kleiger G, Deshaies RJ. (2006). Evaluation of a Diffusion-Driven Mechanism for Substrate Ubiquitination by the SCF-Cdc34 Ubiquitin Ligase Complex. *Molecular Cell.* 24: 523-534.

Pierce NW, Kleiger G, Shan SO, Deshaies RJ (2009). Detection of sequential polyubiquitylation on a millisecond timescale. *Nature.* 462(7273):615-9.

Popp MW, Antos JM, Ploegh HL (2009). Site-specific protein labeling via sortase-mediated transpeptidation. *Curr Protoc Protein Sci. Chapter 15:Unit 15.3.*

Ravid, T. and M. Hochstrasser (2007). Autoregulation of an E2 enzyme by ubiquitin-chain assembly on its catalytic residue. *Nat Cell Biol.* 9: 422-427.

Saha A, Deshaies RJ (2008). Multimodal Activation of the Ubiquitin Ligase SCF by Nedd8 Conjugation. *Mol Cell.* 32: 21-31.

Schmidt MW, McQuary PR, Wee S, Hofmann K, Wolf DA (2009). F-box-directed CRL complex assembly and regulation by the CSN and CAND1. *Mol Cell.* 35(5):586-97.

Schoenheimer R, Ratner S, Rittenberg D. (1939). Studies in Protein Metabolism: X. The Metabolic Activity of Body Proteins Investigated with l (-)-Leucine Containing Two Isotopes*. J Biol Chem.* 130, 703–732.

Schulman BA, Carrano AC, Jeffrey PD, Bowen Z, Kinnucan ER, Finnin MS, Elledge SJ, Harper JW, Pagano M, Pavletich NP (2000). Insights into SCF ubiquitin ligases from the structure of the Skp1-Skp2 complex. *Nature.* 408(6810):381-6.

Siergiejuk E, Scott DC, Schulman BA, Hofmann K, Kurz T, Peter M (2009). Cullin neddylation and substrate-adaptors counteract SCF inhibition by the CAND1-like protein Lag2 in Saccharomyces cerevisiae. *EMBO J.* 28(24):3845-56.

Strohmaier H, Spruck CH, Kaiser P, Won KA, Sangfelt O, Reed SI. (2001). Human F-box protein hCdc4 targets cyclin E for proteolysis and is mutated in a breast cancer cell line. *Nature.* 413: 316-22.

Thrower JS, Hoffman L, Rechsteiner M, Pickart CM. (2000). Recognition of the polyubiquitin proteolytic signal. *EMBO J.* 19: 94-102.

VanDemark AP, Hofmann RM, Tsui C, Pickart CM, Wolberger C (2001). Molecular insights into polyubiquitin chain assembly: crystal structure of the Mms2/Ubc13 heterodimer. *Cell.* 105(6):711-20.

Wilkinson KD, Urban MK, Haas AL. (1980). Ubiquitin is the ATP-dependent proteolysis factor I of rabbit reticulocytes. *J Biol Chem.* Aug 25;255(16):7529-32.

Zhang W, Ito H, Quint M, Huang H, Noël LD, Gray WM (2008). Genetic analysis of CAND1-CUL1 interactions in Arabidopsis supports a role for CAND1-mediated cycling of the SCFTIR1 complex. *Proc Natl Acad Sci U S A.* 105(24):8470-5.

Zheng J, Yang X, Harrell JM, Ryzhikov S, Shim EH, Lykke-Andersen K, Wei N, Sun H, Kobayashi R, Zhang H (2002). CAND1 binds to unneddylated CUL1 and regulates the formation of SCF ubiquitin E3 ligase complex. *Mol Cell.* 10(6):1519-26.